Paleoceanography and Paleoclimatology®

Key Points:

- In the early and middle Miocene simulations, Atlantic overturning is weaker than today; Southern Ocean overturning is dominant over North
- Surface freshwater fluxes controlled the choice of the northern hemisphere basin with overturning
- Lower orography in the Miocene simulations may have favored a Pacific overturning over an Atlantic overturning

Author Contributions:

Conceptualization: Trusha J. Naik, Agatha M. de Boer, Helen K. Coxall
Data curation: Trusha J. Naik, Natalie J. Burls
Formal analysis: Trusha J. Naik
Funding acquisition: Agatha M. de Boer
Project administration: Agatha M. de Boer
Resources: Agatha M. de Boer, Catherine D. Bradshaw, Yannick Donnadieu, Alexander Farnsworth, Amanda Frigola, Nicholas Herold, Matthew Huber, Gregor Knorr, Allegra N. LeGrande, Yousheng Li, Gerrit Lohmann, Daniel J. Lunt, Matthias Prange
Software: Trusha J. Naik, Natalie J. Burls

Ocean Meridional Overturning Circulation During the Early and Middle Miocene

Trusha J. Naik[1,2] ⓘ, Agatha M. de Boer[1,2] ⓘ, Helen K. Coxall[1,2] ⓘ, Natalie J. Burls[3] ⓘ, Catherine D. Bradshaw[4,5] ⓘ, Yannick Donnadieu[6], Alexander Farnsworth[7,8] ⓘ, Amanda Frigola[9,10] ⓘ, Nicholas Herold[11], Matthew Huber[12], Mehdi Pasha Karami[13] ⓘ, Gregor Knorr[14] ⓘ, Allegra N. LeGrande[15,16] ⓘ, Yousheng Li[7], Gerrit Lohmann[10,14] ⓘ, Daniel J. Lunt[7] ⓘ, Matthias Prange[10] ⓘ, and Yurui Zhang[17] ⓘ

[1]Department of Geological Sciences, Stockholm University, Stockholm, Sweden, [2]Bolin Centre for Climate Research, Stockholm, Sweden, [3]Department of Atmospheric, Oceanic and Earth Sciences, Center for Ocean-Land Atmosphere Studies, George Mason University, Fairfax, VA, USA, [4]The Global Systems Institute, University of Exeter, Exeter, UK, [5]Met Office Hadley Centre, Exeter, UK, [6]CNRS, IRD, Coll France, INRA, CEREGE, Aix Marseille University, Aix en Provence, France, [7]School of Geographical Sciences, University of Bristol, Bristol, UK, [8]Tibetan Plateau Earth System, Environment and Resources (TPESER), Institute of Tibetan Plateau Research, Chinese Academy of Sciences, Beijing, China, [9]Barcelona Supercomputing Center, Barcelona, Spain, [10]MARUM – Center for Marine Environmental Sciences, University of Bremen, Bremen, Germany, [11]School of Life and Environmental Sciences, The University of Sydney, Sydney, NSW, Australia, [12]Department of Earth, Atmospheric, and Planetary Sciences, Purdue University, West Lafayette, IN, USA, [13]Rossby Centre, Swedish Meteorological and Hydrological Institute, Norrköping, Sweden, [14]Alfred Wegener Institute Helmholtz Centre for Polar and Marine Research, Bremerhaven, Germany, [15]NASA Goddard Institute for Space Studies, New York, NY, USA, [16]Center for Climate Systems Research, Columbia University, New York, NY, USA, [17]State Key Laboratory of Marine Environmental Science, College of Ocean & Earth Sciences, Xiamen University, Xiamen, China

Abstract The Miocene (~23–5 Ma) is a past warm epoch when global surface temperatures varied between ~5 and 8°C warmer than today, and CO_2 concentration was ~400–800 ppm. The narrowing/closing of the tropical ocean gateways and widening of high-latitude gateways throughout the Miocene is likely responsible for the evolution of the ocean's overturning circulation to its modern structure, though the mechanisms remain unclear. Here, we investigate early and middle Miocene ocean circulation in an opportunistic climate model intercomparison (MioMIP1), using 14 simulations with different paleogeography, CO_2, and vegetation. The strength of the Southern Ocean-driven Meridional Overturning Circulation (SOMOC) bottom cell is similar in the Miocene and Pre-Industrial (PI) but dominates the Miocene global MOC due to weaker Northern Hemisphere overturning. The Miocene Atlantic MOC (AMOC) is weaker than PI in all the simulations (by 2–21 Sv), possibly due to its connection with an Arctic that is considerably fresher than today. Deep overturning in the North Pacific (PMOC) is present in three simulations (~5–10 Sv), of which two have a weaker AMOC, and one has a stronger AMOC (compared to its PMOC). Surface freshwater fluxes control northern overturning such that the basin with the least freshwater gain has stronger overturning. While the orography, which impacts runoff direction (Pacific vs. Atlantic), has an inconsistent impact on northern overturning across simulations, overall, features associated with the early Miocene—such as a lower Tibetan Plateau, the Rocky Mountains, and a deeper Panama Seaway—seem to favor PMOC over AMOC.

Plain Language Summary During the Miocene epoch, which lasted from 23 to 5 million years ago, global temperatures were warmer, and CO_2 levels were higher than they are today. Ocean circulation began evolving toward its modern structure during this period, likely due to numerous tectonic changes, such as the opening and closing of oceanic gateways. However, the exact progression of these changes is still unclear. We use multiple climate models to investigate the factors that influenced ocean circulation during the Miocene. Our findings show that, in the Southern Ocean, deep circulation was similar to today, while it was weaker in the North Atlantic. Some Miocene simulations indicate deep circulation in the North Pacific, a feature not present today. Surface freshwater flux controlled whether deeper circulation occurred in the North Atlantic or the North Pacific. The height of mountain ranges, such as the Tibetan Plateau and the Rocky Mountains, may have also played a role: lower mountains may have favored deep circulation in the Pacific. Overall, early Miocene features, like a deeper Panama Seaway and lower mountains, appear to support deep circulation in the Pacific rather than the Atlantic.

Supervision: Agatha M. de Boer, Helen K. Coxall
Visualization: Trusha J. Naik
Writing – original draft: Trusha J. Naik, Agatha M. de Boer
Writing – review & editing: Trusha J. Naik, Agatha M. de Boer, Helen K. Coxall, Natalie J. Burls, Catherine D. Bradshaw, Yannick Donnadieu, Alexander Farnsworth, Amanda Frigola, Nicholas Herold, Matthew Huber, Mehdi Pasha Karami, Gregor Knorr, Allegra N. LeGrande, Yousheng Li, Gerrit Lohmann, Daniel J. Lunt, Matthias Prange, Yurui Zhang

1. Introduction

The Miocene (∼23.0–5.3 Ma) was a highly dynamic warm epoch of the Neogene Period, which is further divided into the early Miocene (23–16 Ma), the middle Miocene (mid-Miocene; 16–11.6 Ma), and the late Miocene (11.6–5.3 Ma). The mid-Miocene, a period of relative warmth, also coincided with a warm period called the Miocene Climatic Optimum (MCO; 16.9–14.7 Ma). This was followed by an abrupt cooling phase, known as the mid-Miocene Climate Transition (MMCT; 14.7–13.8 Ma) when the Antarctic Ice Sheet expanded and a permanent ice sheet was established on East Antarctica (Miller et al., 2020). The modern ocean circulation pattern, with a dominant North Atlantic deep-water formation, might have initiated as early as the Eocene (∼47 Ma) or at the Eocene-Oligocene transition (EOT; ∼34 Ma) and strengthened in the Miocene, as suggested by multiple proxies, including drift deposits, Nd isotopes, biomarkers and stable carbon isotopes, which point to a strengthening of deep-water formation in North Atlantic from the late Oligocene (∼25 Ma) to Miocene (Abelson & Erez, 2017; Borrelli et al., 2014; Boyle et al., 2017; Langton et al., 2016; Scher & Martin, 2008; Uenzelmann-Neben & Gruetzner, 2018; H. Wang et al., 2023; J. D. Wright & Miller, 1996). Thus, the Miocene is an important and dynamic time in terms of the drivers of modern ocean circulation patterns.

Changes in paleogeography (with all other forcings removed) play a major role in driving ocean circulation at geologic timescales, for example, over the Cretaceous and Eocene (Farnsworth et al., 2019; Lunt et al., 2016). During the Miocene, numerous tectonic changes took place (Potter & Szatmari, 2009). The Panama Seaway constricted throughout the Miocene and possibly shoaled to critical depths for Pacific-Atlantic deepwater exchange between 11 and 9 Ma (Kirillova et al., 2019; Osborne et al., 2014). The Tethys Seaway closed sometime in the middle Miocene, ending low latitude exchange between the Indian and Atlantic oceans (Bialik et al., 2019; Sun et al., 2021). The Fram Strait widened and deepened from the early to middle Miocene, between ∼20 and 17 Ma, allowing for a bidirectional flow between the North Atlantic and Arctic Oceans (Hossain et al., 2020, 2021; Jakobsson et al., 2007). Significant continental tectonic activity also occurred during the Miocene (Potter & Szatmari, 2009). The Rocky Mountains may have been higher before the Miocene and lowered to modern elevations (1,800 to 4,400 m; Madole et al., 1987) by the middle Miocene (Chamberlain et al., 2012; Wolfe et al., 1997). The Tibetan Plateau started uplifting before the Miocene, likely with regional variability and asynchrony as the orogeny progressed (Ding et al., 2022; C. Wang et al., 2014). These major changes in the oceanic gateways and orography affected ocean circulation by changing the path of the ocean currents and the geometry of runoff, thus affecting the salinity of the deepwater formation regions (Hamon et al., 2013; Maffre et al., 2018; Schmittner et al., 2011; Steph et al., 2006).

Several Miocene simulations have been performed in coupled climate models thus far (e.g., Bradshaw et al., 2012, 2015; Brierley & Fedorov, 2016; Crichton et al., 2021; Frigola et al., 2021; Hamon et al., 2013; Herold et al., 2011; Huang et al., 2017; Knorr & Lohmann, 2014; Micheels et al., 2009, 2011; Pillot et al., 2022). However, many of these studies focus traditionally on the impact of CO_2 or paleogeography on the atmosphere rather than the ocean (e.g., Goldner et al., 2014; Knorr et al., 2011; Micheels et al., 2009). When ocean circulation is mentioned, it is often confined to the Atlantic (Pillot et al., 2022) or the Southern Ocean (Huang et al., 2017). The ocean circulation is sometimes studied with a specific interest in the impact of a strait and then does not always include a complete Miocene topography and bathymetry (von der Heydt & Dijkstra, 2006). For the few studies that have described the circulation, the results are conflicted, with some studies suggesting that the Atlantic branch of the Meridional Overturning Circulation (MOC), commonly abbreviated as AMOC, had strengthened after the shoaling of the Panama Seaway (Brierley & Fedorov, 2016; Butzin et al., 2011; Lunt et al., 2008) while others find a strong AMOC in the Miocene with a wide-open seaway (Krapp & Jungclaus, 2011). Similarly, the role of the closure of the Tethys is also questioned, as one study found that the closure of the Tethys Seaway has a profound impact on the AMOC (Z. Zhang et al., 2011), while another study found that the change in transport due to the closure of the Tethys Seaway does not affect the circulation as much as the presence of a Greenland Ice Sheet (Pillot et al., 2022). As a result, there is no clear picture of what Miocene climate model simulations suggest for ocean circulation (Steinthorsdottir et al., 2021). Furthermore, previously, there has been only one multi-model ocean intercomparison study relevant to the Miocene, focusing on the effect of paleogeography on ocean circulation, which was produced for the early Eocene (Y. Zhang et al., 2022).

Here, we use an opportunistic coupled-climate-model intercomparison of 14 simulations, made available through the informal MioMIP1 (Burls et al., 2021), and focus specifically on the behavior of the ocean circulation and the role of paleogeography in the warmer early and middle Miocene. An earlier study of the MioMIP1 ensemble,

focusing on the surface temperature, found that CO_2 is the main factor controlling Miocene warmth, with other factors such as the paleogeography and reduced ice sheets playing a secondary but non-negligible role in increasing the global mean temperature (Burls et al., 2021). Paleogeography, through ocean and atmospheric circulation changes, impacts heat transport, carbon cycle feedbacks, and regional climate (Fyke et al., 2015; Hossain et al., 2020; Sijp et al., 2014), though carbon cycle feedbacks are not included in the MioMIP1 simulations. The advantage of this informal MIP, compared to a formally designed MIP with specified boundary conditions, is that the models sample a wide spectrum of potential Miocene paleogeographies and thus explore a larger spectrum of uncertain boundary conditions. The disadvantage is that the simulations were mostly executed independently, so there are no control studies that facilitate "open-close gateway" comparisons. Nor can we robustly determine whether the different paleoclimate model physics are driving the observed changes rather than the different paleogeographies (or a combination of both). Nevertheless, we attempt to identify commonalities in the role of certain geographic features on ocean circulation and discuss these within the context of other influencing factors. So as not to complicate the comparison further, we have chosen to focus on those simulations with a similar atmospheric CO_2 (i.e., in the range of 355–760 ppm) and only those simulations targeting early and middle Miocene periods. The impact of CO_2 on climate in MioMIP1 is the focus of Burls et al. (2021) and the impact on the hydrological cycle is examined in Acosta et al. (2024). Here, we focus on the impact of paleogeography on the MOC and attempt to summarize the results in terms of possible scenarios for the evolution of the ocean circulation throughout the Miocene.

In Section 2, we describe the simulations and methods used in this study. The deep overturning circulation is described in Section 3, and its drivers in Section 4, followed by a summary of some available proxies in Section 5. In Section 6, we investigate discrepancies between the calculated and target ages of each simulation, and finally, we discuss the results and draw conclusions in Section 7.

2. Data and Methods

2.1. Models

We use 14 simulations in this study, carried out with seven fully coupled Earth System Models simulating the Miocene using a range of boundary conditions (Table 1, Figure 1). Of the seven models, 6 (CCSM3, CCSM4, CESM1, COSMOS, IPSLCM5, HadCM3L) are described in detail in Burls et al. (2021) as well as 9 of the 14 simulations. A detailed description of GISS-E2.1 model components and physics is provided in Kelley et al. (2020). The remaining five simulations not included in Burls et al. (2021) are new additions to the MIP of opportunity ensemble as described below.

The nine simulations that are described in Burls et al. (2021) are as follows; CCSM3_F, COSMOS, HadCM3L_B1, HadCM3L_B2 (HadCM3L-Bradshaw), HadCM3L_F1, HadCM3L_F3 (HadCM3L-Farnsworth), CCSM3_H (CCSM3-NH3), CCSM4, CESM1 (CESM1-CAM5). For the simulations where a different naming convention is used in this study, their naming as per Burls et al. (2021), is given in the brackets next to the names used in this study. The details of all the simulations are given in Table 1. The pre-industrial simulation for CESM1-CAM5 was not available through the MioMIP1 database thus it is taken from J. Zhu et al. (2019).

Two of the five new simulations used in this study, HadCM3L_F2 and HadCM3L_L1, were conducted with the HadCM3L model. The model components used here are the same as HadCM3L_F1 and F3, the difference lies in the boundary conditions. HadCM3L_F2 has the same paleogeography as F1 (Figures 1i and 1j), which is provided by Getech Plc., but the CO_2 level is higher at 760 ppm to match the recent estimates of Rae et al. (2021). HadCM3L_L1 uses the same model components, but the paleogeographic boundary conditions are as described in Scotese and Wright (2018), with a CO_2 level of 494 ppm. The GISS-E2.1 simulation targets the MCO, using the paleogeographic boundary conditions described in Frigola et al. (2018), and the CO_2 is 456 ppm. The final two new simulations, IPSLCM5 and IPSLCM5_T, are produced using the IPSLCM5 model. A description of the IPSLCM5 model components is provided in Burls et al. (2021), who use differently configured IPSLCM5 Miocene simulations; further details are provided in Pillot et al. (2022). Both the simulations have no Greenland Ice Sheet with an intermediate open Panama Seaway with a depth of 400 m (Figures 1e and 1f). The difference is in the Tethys Seaway, which is closed for IPSLCM5 and open and shallow (120 m deep) for IPSLCM5_T.

Table 1
The Specifications of Each Miocene Simulation Used in This Study

Model	Resolution (Atm/Ocn)	Length (years analyzed)	Initial conditions	CO₂ (ppm)	Paleogeography	Ice sheets	Depth of seaways	Target time period	Reference
CCSM4	~1.9° × 2.5°/1°	2000 (last 100)	Continued from CCSM3_H Mid-Miocene simulation used in this study	400	Herold et al. (2011) (updated)	GIS ~ 0.9 m SLE, AIS ~ 20 m SLE	PS: 3,751 m, ETS: 180 m, FS: 2,768 m	20–14 Ma	Burls et al. (2021)
CESM1	~1.9° × 2.5°/1°	3000 (last 50)		400	Herold et al. (2011) (updated)	GIS ~ 0.9 m SLE, AIS ~ 20 m SLE	PS: 3,751 m, ETS: 180 m, FS: 2,768 m	20–14 Ma	Burls et al. (2021)
CCSM3_H	T31–3.75°/~3° × 1.5°	1100 (last 100)	Modern global depth averaged salinity and temperature	355	Herold et al. (2011)	Herold et al. (2008); AIS height reduced by 1,000 m	PS: 3,030 m, ETS: 2,555 m, FS: 1,280 m	20–14 Ma	Herold et al. (2011)
CCSM3_F	T42–2.8°/1°	1500 (last 100)	Temperature: Reduces from 19° to 9°C from surface to 500 m and 9°C below that. Salinity: 35 PSU everywhere	400	Frigola et al. (2018)	No GIS, AIS ~ 16 m SLE	PS: 514 m, ETS: 4,000 m, FS: 1,500 m	16.7–14.5 Ma (MMCO)	Frigola et al. (2018)
COSMOS	3.75° × 3.75°/~3°	2000 (last 100)	Zonal mean of temperature and salinity taken from the World Ocean Atlas (1994; (Levitus & Boyer, 1994; Levitus et al., 1994))	450	Herold et al. (2011) + NA/Arctic reconstruction (Ehlers & Jokat, 2013)	No GIS, AIS - Herold et al. (2008)	PS: 3,395 m, ETS: 2,525 m, FS: 1,885 m	20–14 Ma	Stärz et al. (2017)
HadCM3L_B1	3.75° × 2.5°	2000 (last 50)	Continued from 2100 years Late Miocene simulations	400	Markwick (2007)	No GIS, No AIS	PS: 995 m, ETS: Closed, FS: 1,500 m	15.9–11.6 Ma (Mid-Miocene)	Bradshaw et al. (2021)
HadCM3L_B2	3.75° × 2.5°			400		No GIS, AIS - 55 m SLE			
HadCM3L_F1	3.75° × 2.5°/3.75° × 2.5°	7422 (last 100)	Homogeneous global ocean salinity and an idealized zonal mean ocean temperature structure as a cosine function of latitude (Lunt et al., 2016)	400	Getech Plc.	AIS, No GIS	PS: 995 m	15.9–13.8 Ma (Langhian)	Farnsworth et al. (2019)
HadCM3L_F2				760			ETS: Closed, FS: 995 m	15.9–13.8 Ma (Langhian)	
HadCM3L_F3				400			PS: 995 m, ETS: Closed, FS: 1,500 m	13.8–11.6 Ma (Serravallian)	
HadCM3L_L1			Continued from 3000-year Mid-Miocene run	494	Scotese and Wright (2018)		PS: 2,731 m, ETS: Closed, FS: 1,500 m	15.9–13.8 Ma (Langhian)	–

Table 1
Continued

Model	Resolution (Atm/Ocn)	Length (years analyzed)	Initial conditions	CO$_2$ (ppm)	Paleogeography	Ice sheets	Depth of seaways	Target time period	Reference
IPSLCM5	3.75° × 1.875°/ 2°–0.5°	3000 (last 100)	Uniform salinity of 34.7 PSU. Zonal SST gradient—from 34 to 10°C and deep ocean at 6°C	560	Poblete et al. (2021)	AIS, no GIS, Tethys 120 m	PS: 1,033 m ETS: Closed FS: 272 m	20 Ma	Pillot et al. (2022)
IPSLCM5_T				560		AIS, no GIS, Tethys closed	PS: 1,033 m ETS: 120 m FS: 272 m	20 Ma	
GISS-E2.1	2° × 2.5°/ 1° × 1.25°	5000 (last 100)	Zonal averages of temperature and salinity from World Ocean Atlas 2001 (Boyer & Levitus, 2002; Stephens & Levitus, 2002)	456	Frigola et al. (2018)	No GIS, AIS ∼ 16 m SLE	PS: 1,214 m ETS: 4,009 m FS: 2,677 m	16.7–14.5 Ma (MMCO)	—

Note. AIS, Antarctic Ice Sheet; GIS, Greenland Ice Sheet; PS, Panama Seaway; ETS, Eastern Tethys Seaway; FS, Fram Strait.
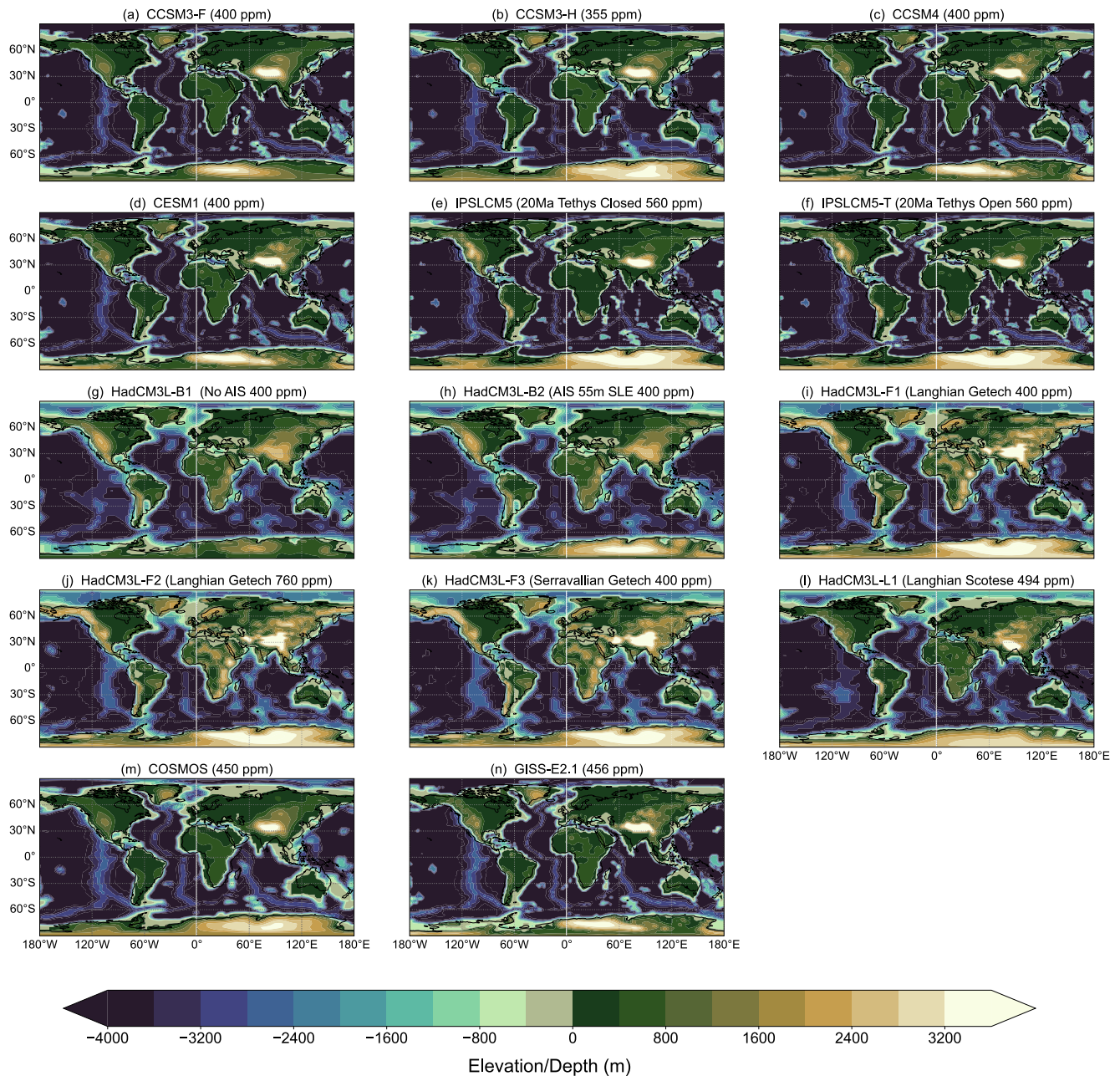
Figure 1. Topography and bathymetry (m) of the Miocene simulations. Black outline indicates modern coastlines.

2.2. Overturning Streamfunction

The meridional overturning streamfunction represents the zonally integrated circulation in the meridional plane of a basin or the global ocean. It gives an idea of the latitudinal location of deep-water formation (downwelling) and upwelling. Of the 14 simulations, 9 have the meridional overturning streamfunctions available as the model output. These simulations are; HadCM3L_B1, HadCM3L_B2, HadCM3L_F1, HadCM3L_F2, HadCM3L_F3, HadCM3L_L1, COSMOS, IPSLCM5 and IPSLCM5_T. For the remaining simulations (CCSM3_F, CCSM3_H, CCSM4, CESM1, and GISS-E2.1), we calculated the streamfunction using the available meridional velocities. We use the Eulerian Mean Streamfunction, which is calculated by integrating the meridional velocities zonally and then vertically to obtain the 2D structure of the ocean circulation:

$$\psi(y,z) = \int\limits_{-z}^{0} \int\limits_{x_e}^{x_w} v(x,y,z')\,dx\,dz'$$

where $\psi(y,z)$ is the meridional streamfunction and $v(x,y,z')$ is the meridional velocity integrated from west to east and top to bottom. We use the annual averaged velocity values as those are the ones available for all the simulations. The Eulerian mean is due to the mean advection and does not account for the mesoscale and sub-mesoscale eddies and the bolus velocity, which are particularly important in the ACC region (Rintoul et al., 2001; Yang et al., 2015). These regimes are not included within the regions where we focus on the maximum overturning so our Eulerian streamfunction should be sufficient for the purposes of this study. The Atlantic Meridional streamfunction is calculated by applying a basin mask over the data that excludes the Pacific and Indian Oceans. In this study, we combine the Indian and Pacific streamfunctions and refer to this as the Pacific Streamfunction. The maximum overturning in the upper cells in the North Atlantic (AMOC) and North Pacific (PMOC) is calculated as the maximum positive streamfunction north of the equator, below 400 m depth, to exclude the wind-driven gyre circulation. The Southern Ocean overturning (SOMOC) is defined as the largest negative value in the global MOC (GMOC) streamfunction below 1,000 m, that is, the largest negative value of the bottom cell. For comparison, we also define the local overturning cell in the Southern Ocean, which is calculated as the maximum negative value of GMOC streamfunction south of 60°S. This southern cell is sometimes used as an indication of the strength of the bottom cell but as we shall see, they are not correlated. The latitudinal and depth extents of AMOC, PMOC, and SOMOC (bottom cell) are provided in Table S3 in Supporting Information S1.

2.3. Freshwater Transports and Surface Freshwater Flux

The volume of liquid freshwater transport across the Fram Strait is calculated to understand how the freshwater export from the Arctic affects the circulation in the North Atlantic. The formula for freshwater transport is taken from Li et al. (2017). The resultant freshwater transport can be interpreted as the necessary volume of water to balance the salinity flux across the strait cross-section,

$$\text{FWT} = -\int\limits_{-h}^{0} \int\limits_{x_w}^{x_e} v(x,z) \times \frac{S(x,z) - \overline{S}}{\overline{S}}\,dx\,dz$$

where $\overline{S}$ is the reference salinity, which in this study is the area-weighted salinity of the strait cross-section, $v(x,z)$ is the meridional velocity and $S(x,z)$ is the salinity of each grid box along the cross-section. In each case, the cross-section selected is the narrowest section between the North Atlantic and the Arctic Ocean. $S(x,z)$ and $v(x,z)$ are annual means and hence, only represent the mean flow, neglecting the salinity transport by eddies.

The surface freshwater flux (FWF) received by the North Atlantic and North Pacific is calculated using the formula, FWF = Precipitation-Evaporation + Runoff, where FWF is the area-weighted average freshwater flux above 40°N in both basins.

2.4. Target Age of Simulations

In this study, we attempt to identify the discrepancies between the target ages of the simulations and the age ranges they actually represent with their paleogeography. For that purpose, we need to assign a paleogeographic age (or range) to each simulation. The simulations all have an assumed age (range) that they represent, but the paleogeographies associated with similar ages can be different, the target age range can be broad, and simulations can be sensitivity studies that used a control simulation in one age but test the sensitivity of a strait in a different period. For example, models using paleogeography described in Herold et al. (2011) simulate the Miocene for a broad range from 14 to 20 Ma. The IPSLCM5 simulations have an essentially closed Fram Strait, placing it in the early Miocene, but also a closed or narrow Tethys, and restricted Panama Gateway more associated with the late Miocene from a paleogeographic-evolution perspective. Therefore, it cannot realistically be associated with a

specific sub-age of the Miocene. To account for these uncertainties, we here provide our estimate of the range of ages that each simulation represents (Figure 12, Table S1 in Supporting Information S1).

We base our age estimate on the cross-sectional area of the three straits that opened or closed during the Miocene, namely the Tethys Seaway, Panama Gateway, and the Fram Strait. Given the large uncertainties in the timing of the evolution of the width and depth of the straits, it is problematic to assign a specific age to each simulation. Nevertheless, a rough estimate is a useful start as long as the large uncertainties are always kept in mind when interpreting the results. For each of the three straits, we derive a linear relationship between cross-section and age using two pairs of (cross-section, age) end members. The cross-section end members are assumed to be the widest and closed or shallowest cross section in all the simulations, and as age end members, we assign ages using the estimates from Figure 3 of Ferreira et al. (2018) (Figure S1 in Supporting Information S1) and other studies that provide more distinct estimates.

Specifically, for the Fram Strait, which was likely shallow before the mid-Miocene (Jakobsson et al., 2007), we placed the simulations with the smallest cross-sectional area of 4×10^7 m^2, IPSLCM5, and IPSLCM5_T, at 21 Ma (based on Jakobsson et al. (2007) and Jokat et al. (2016)) and the simulations with the largest area of 4.7×10^8 m^2, COSMOS, at 10 Ma, when the strait is thought to be completely open (Figure S1 in Supporting Information S1). Using this equation, each simulation is then assigned an age according to its Fram Strait cross-section. We then add two more age estimates from the other two straits.

The important phases of Panama Seaway closure are typically considered to have occurred in the late Miocene and Pliocene (Osborne et al., 2014; Webb, 2006). Some studies suggest that the Atlantic-Pacific oceanic flow relevant to AMOC behavior had effectively ceased as early as the middle Miocene (Montes et al., 2012, 2015), although this has been challenged (Kirillova et al., 2019; Osborne et al., 2019; O'Dea et al., 2016). In this study, since the Panama Seaway is not closed in any simulations, we place the simulation with the smallest area of the seaway, CCSM3_F (6.28×10^7 m^2) at 9 Ma according to Kirillova et al. (2019), when the seaway is proposed to have experienced a critical shoaling step. The largest cross-section area of Panama Seaway is 1.5×10^9 m^2 for COSMOS, and hence, it is placed at 17 Ma (as per Figure S1 in Supporting Information S1), but the age could be any time before that since it first started constricting around 17 Ma. Using these two endpoints, we calculate the ages for the rest of the simulations.

The timing of closure of the Eastern Tethys Seaway (referred to as the Tethys Seaway in this study) is also highly debated, with closure ages ranging from ~35 to 34 Ma (Allen & Armstrong, 2008; C. Wang et al., 2002) to a middle Miocene closure of ~14-13 Ma (Hamon et al., 2013; Sun et al., 2021). The Tethys Seaway is shown to close around 10 Ma in Figure S1 in Supporting Information S1. However, recent studies have shown that the seaway likely closed completely by ~13.8 Ma (Bialik et al., 2019) or ~12.8 Ma (Sun et al., 2021). We use these dates to place the simulations with a closed Tethys Seaway (HadCM3L_B1, B2, F1, F2, F3, L1, and IPSLCM5) at 13 Ma, but it could represent an age any time after 13 Ma. The simulation (GISS-E2.1) with the largest area is placed at 18 Ma when the Tethys Seaway was thought to be completely open (Figure S1 in Supporting Information S1). The resulting age estimates for each model, calculated for all three gateways, are given in Table S1 in Supporting Information S1.

3. Deep Ocean Circulation

The geographical location of deep water formation is indicated by a deep mixed layer depth (MLD) (e.g., Y. Zhang et al., 2022). Observations and numerical experiments have shown that winter-time cooling at high latitudes increases surface water density, and this densification is augmented by brine rejection during sea-ice formation. This leads to deep convection and the formation of deep mixed layers during the winter (Jacobs, 2004; Marshall & Schott, 1999; Pellichero et al., 2017; Våge et al., 2009). Here, we show the annual MLD for the Miocene simulations (rather than the winter MLD) since this is the output available for all simulations (Figure 2). The winter MLD would be deeper, as that is when deep convection occurs. We chose a cut-off of 300 m for the annual MLDs to define regions with persistent deep-water formation, as that provides a good overview of the spatial distribution of polar and subpolar MLDs. Choosing a deeper cut-off (>300 m) does not affect the location of deepwater formation. However, it excludes some deep MLD regions in a few models. It should be noted that it is not possible to directly compare the MLD across models due to the implementation of different criteria and methods for defining MLD (Treguier et al., 2023). Here, we use the MLD to indicate the basin that is preferred for deep-water formation and the spatial extent of this deep-water formation. This is later
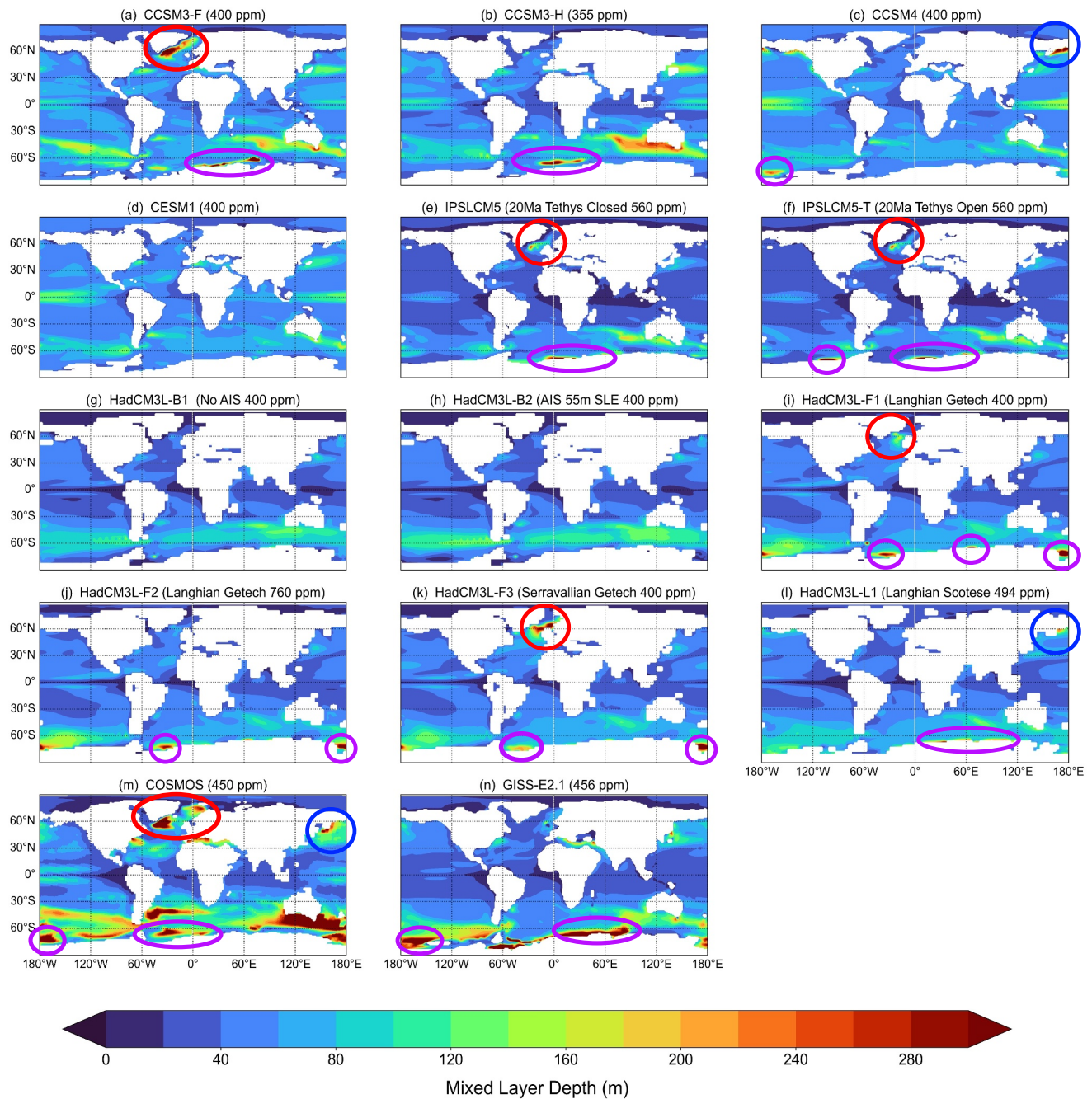
Figure 2. The annual averaged Mixed Layer Depths (MLDs) for the Miocene simulations. The regions circled in red indicate the deep MLDs in the North Atlantic, the blue circles indicate deep MLDs in the North Pacific, and the regions circled in purple indicate deep MLDs in the Southern Ocean. These polar and sub-polar regions with deep mixed layers are regions where convection leads to deep-water formation and gives a spatial overview of the basins supporting open convection.

verified by the meridional overturning streamfunction (see Figures 3–5). The red circles in Figure 2 indicate the regions with deep MLD in the North Atlantic, blue circles indicate the same in the North Pacific, and purple circles indicate deep MLD in the Southern Ocean. Of the 14 Miocene simulations, we have 7 with mixed layer depths deeper than 300 m in the Northern Hemisphere. Of these, 5 have deeper MLD in the Atlantic (Figure 2, red circles), and 3 have MLD deeper than 300 m in the Pacific (Figure 2, blue circles). In the Southern Ocean, 11 of the 14 simulations show deep MLD (Figure 2, purple circles). In the North Atlantic, deep MLDs in most of the Miocene simulation are mainly present in the region south of the Greenland-Scotland Ridge and around S-SE
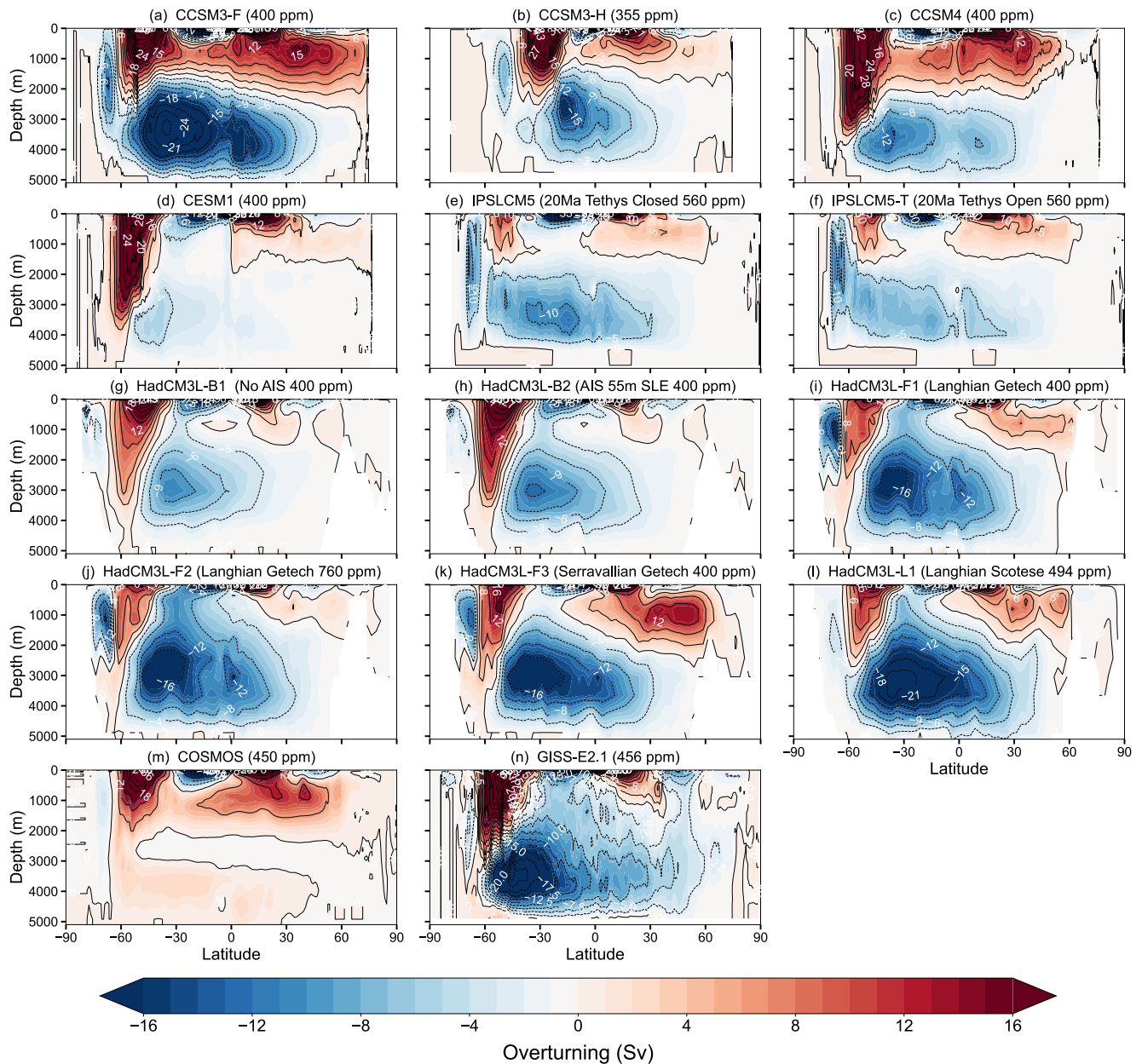
Figure 3. The Global Meridional Overturning Circulation for the Miocene simulations. The red contours indicate clockwise cells, and the blue circles indicate anti-clockwise cells of circulation. The anticlockwise (blue) contours show the overturning strength in the Southern Ocean, and this can be hard to detect in the AMOC and PMOC plots because of the open geographical boundaries in the Southern Ocean.

Greenland. In the PI simulations, the deep MLDs in the North Atlantic are also found in the Nordic Seas in all of the simulations (Figure S2 in Supporting Information S1). In our simulations, the average latitude of deepwater formation in the North Atlantic shifted from 61°N in the Miocene to 65°N in PI.

The MLDs give a spatial overview of regions of deep mixing in the ocean. To investigate the deep circulation, we use the MOC streamfunction (Figures 3, 5, and 6). Note that here, we use the Eulerian mean streamfunction, which is more readily available in the model output repository (see methods). The global MOC (GMOC; Figure 3) is the zonally integrated global overturning and is useful for diagnosing the Southern Ocean MOC (SOMOC), which, by our definition, is the bottom cell driven by Southern Ocean convection. A clockwise circulation (as viewed in a westwards direction through the meridional cross section) is indicated in red (positive values), and an anti-clockwise circulation is indicated in blue (negative values).

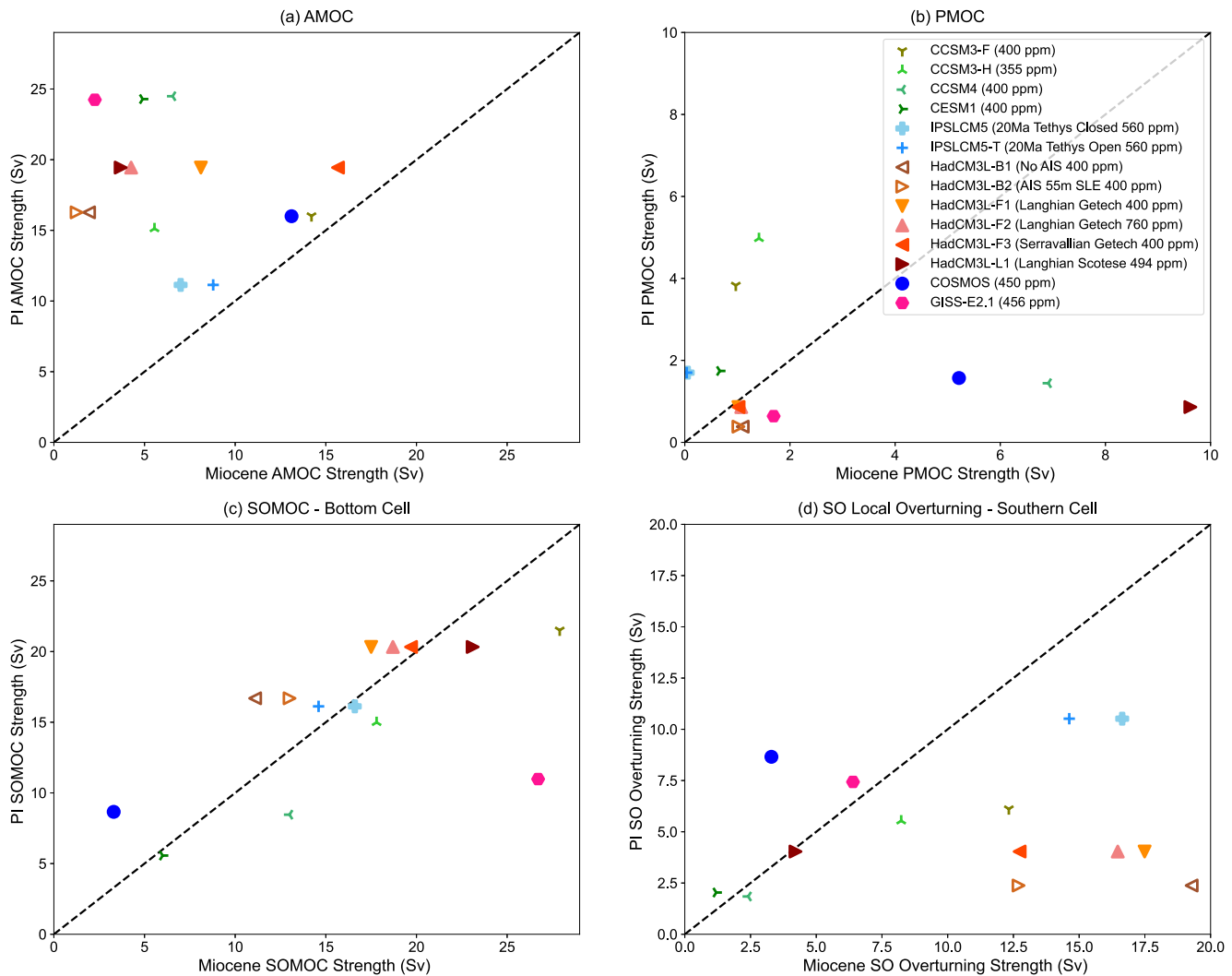**Figure 4.** The strength of the meridional overturning in PI simulations versus the Miocene simulations (in Sv) in (a) North Atlantic (AMOC), (b) North Pacific (PMOC), and (c) Southern Ocean (SOMOC)—Bottom cell and (d) Southern ocean overturning—Southern cell. The definitions of each are given in Section 2.2. The dashed line is the line with slope 1, indicating no change. Simulations to the right and below this line indicate that the overturning is stronger in the Miocene compared to PI for these simulations, and simulations lying to the left and above the line have a stronger PI overturning.

The Global MOC (Figure 3) reveals a stronger SOMOC compared to the MOC in the northern basins in most of the simulations. However, the strength of the SOMOC in the Miocene simulations is similar to that in the Pre-Industrial (PI) simulations (Figure 4c, Table S2 in Supporting Information S1), and it is the overturning in the north that is more different between the time periods (Figures 4a and 4b). The apparent indifference of the SOMOC to the changing climate and boundary conditions is somewhat surprising. This cell is challenging to simulate for several reasons. It is fed by bottom water formed on the Antarctic continental shelf in processes that cannot be resolved in current climate models, where it usually forms in open ocean MLD regions (de Boer et al., 2022; Heuzé, 2020). The return circulation is driven by diapycnal mixing, but again, this is not well constrained, and models parameterize this mixing differently (De Boer & Hogg, 2014). Finally, models are often tuned so that their AMOC cell is in line with observations, but there are no analogous observations of the bottom cell of the ocean to ground truth models. The consequence is that models simulate very different bottom circulation states, as can be seen in our PI simulations where it varies between ∼5 and 22 Sv (Table S2 in Supporting Information S1). This suggests that the SOMOC bottom cell is less sensitive to the surface forcing changes between PI and Miocene than to the different model physics. Indeed, despite an unchanging bottom cell, there is a general tendency for stronger convection in the Southern Ocean during the Miocene, as indicated by deeper MLDs (Figure S3 in Supporting Information S1) and stronger local overturning in the Southern Ocean
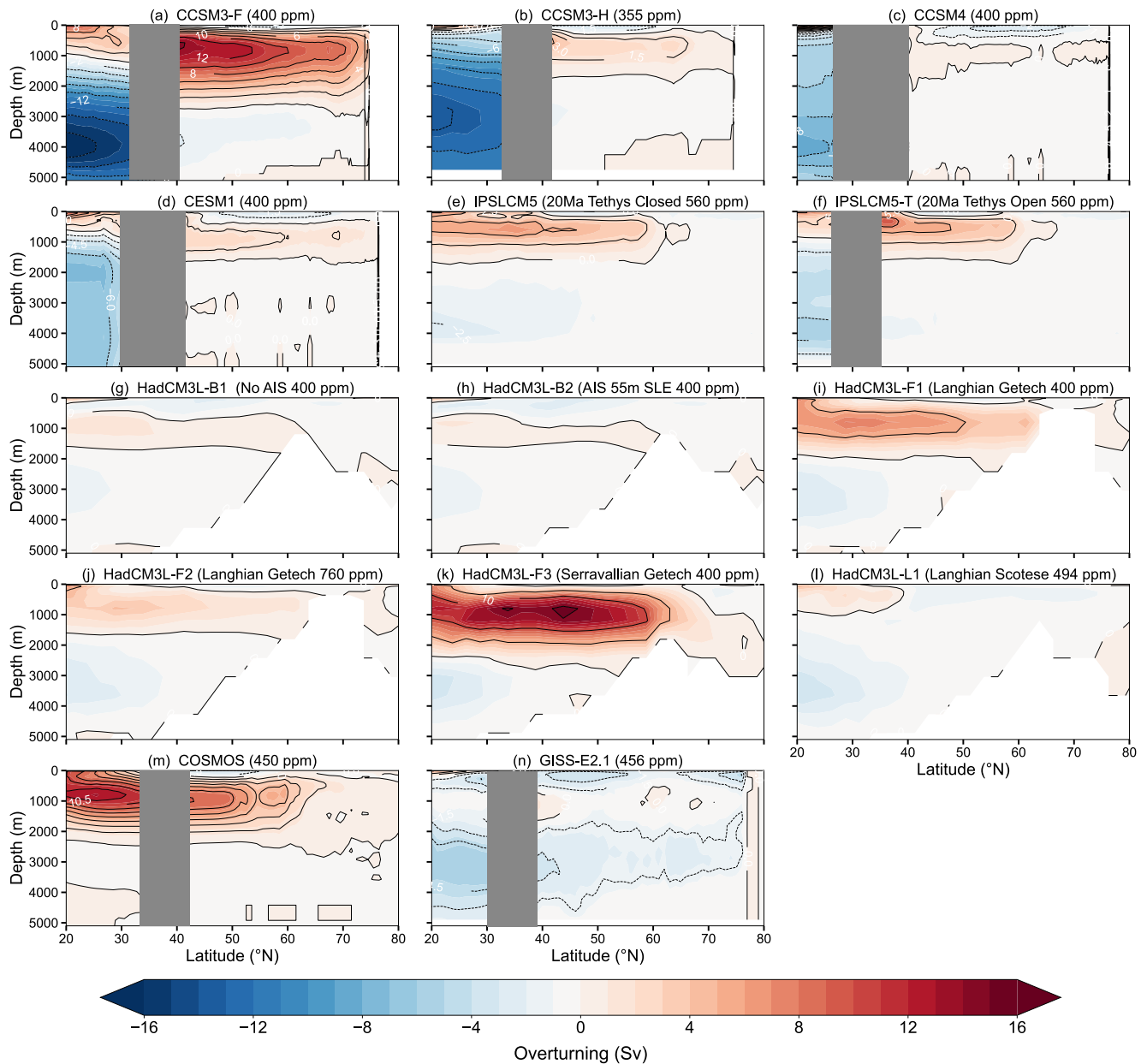
Figure 5. The meridional overturning streamfunctions in the North Atlantic Ocean (AMOC). The latitudes with an open boundary, like the Tethys Seaway and Indonesian Seaway, are blocked out in gray. The white region in panels (g–l) is the bathymetry mask of the HadCM3L simulations. Red contours indicate a clockwise circulation, with sinking in the north and upwelling in the south. Blue contours indicate anticlockwise cells with sinking in the south and upwelling in the north. The units are in Sverdrups (10^6 m^3/s).

(Figure 4d). The higher mean ocean temperatures could contribute somewhat to the stronger overturning here, but it probably does not explain the full signal since the warming is rather modest to have a large impact on the equation of state (de Boer et al., 2007). A cursory investigation of Southern Ocean winds and surface buoyancy forcing did not lead to a robust conclusion either, so a full explanation of strong convection in the Southern Ocean remains beyond the scope of this paper.

As expected, the simulations with deep MLD in the North Atlantic (Figures 2a, 2e, 2f, 2k, and 2m) also have moderately strong overturning cells (Figures 5a, 5e, 5f, 5k, and 5m). The areas with open boundaries (i.e., Tethys and Indonesian Seaways) are blocked out for the basin-specific stream functions since the streamfunction is ill-defined in these regions. Most of the simulations have weak but consistent clockwise overturning in the North
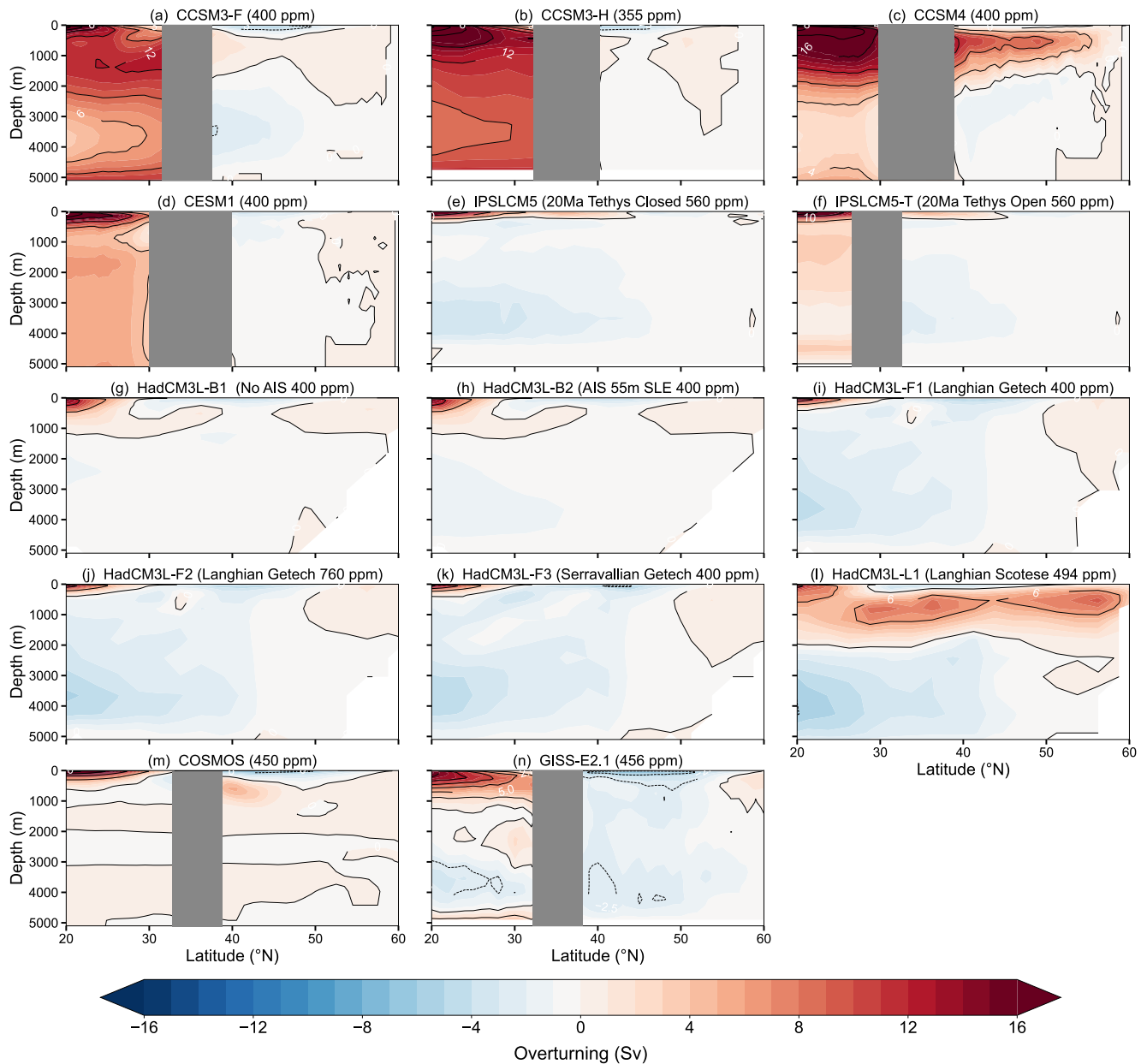
Figure 6. The Pacific Meridional Overturning Circulation (PMOC) north of 20°N is shown here. It is the Indian and Pacific streamfunctions calculated together (Indo-Pacific). We refer to it as the PMOC. The latitude bands with an open boundary, like the Tethys Seaway and Indonesian Seaway, are blocked out in gray. Similar to Figure 3, the red contours indicate clockwise cells, and the blue contours indicate anti-clockwise circulation.

Atlantic up to a depth of ~1,500–2,000 m. Only three simulations ((a) CCSM3_F, (k) HadCM3L_F3, and (m) COSMOS) have a maximum streamfunction above 10 Sv (Table S2 in Supporting Information S1). All the simulations have a weaker AMOC compared to their pre-industrial value (Table S2 and Figure S4 in Supporting Information S1). HadCM3L_F3 shows a stronger AMOC at 60°N due to the northward shift of maximum overturning during the Miocene (Figure S4 in Supporting Information S1).

A similar pattern of consistent overturning is not observed in the Pacific (Figure 6). Only 3 of the 14 simulations show weak clockwise cells up to ~2,000 m, with a Ψ_{max} of ~7 Sv in CCSM4, ~5 Sv in COSMOS and ~10 Sv in HadCM3L_L1. COSMOS has overturning in both the North Atlantic and North Pacific, although the Pacific overturning is weaker than in the Atlantic.

4. Drivers of Overturning

In this section, we explore what controls the deep-water formation in the Northern Hemisphere. We look specifically at the role of surface freshwater flux in the Atlantic, Pacific, and Arctic and the impact of open low-latitude straits and orography.

4.1. Surface Freshwater Flux and Salinity

The surface freshwater flux (FWF) plays a major role in determining the location of deepwater formation in the Northern Hemisphere. In the modern ocean, one of the reasons that there is deepwater formation in the North Atlantic but not in the North Pacific is that the North Pacific receives a higher amount of surface freshwater compared to the North Atlantic (Ferreira et al., 2018). In modern climate model hosing experiments, where excess surface freshwater is gradually supplied to the Arctic and North Atlantic to simulate the impact of the melting of the Greenland Ice Sheet, the AMOC declines substantially with increasing rate of freshwater input (Jackson & Wood, 2018). Similar weakening of the AMOC due to excess surface freshwater input has been reported for paleoclimate simulations and proxies for the Holocene (Morrill et al., 2013) and the Quaternary (Toucanne et al., 2015). The AMOC exhibits increased sensitivity to surface freshwater forcing under Last Glacial Maximum boundary conditions, with a closed Bering Strait (as was the case for the Miocene), which blocks the escape route of excess freshwater into the Pacific through the Arctic (de Boer & Nof, 2004a, 2004b; Pöppelmeier et al., 2021). The Miocene was warmer than today by ∼5–8°C (Steinthorsdottir et al., 2021), and this warmer climate likely led to a stronger hydrological cycle with increased precipitation in the high latitudes compared to modern and different orography impacting the atmospheric freshwater pathways (Acosta et al., 2024; Feakins et al., 2012). As a consequence of this warmth, and because of the nonlinearity of the equation of state, this would enhance the impact of thermal fluxes (i.e., cooling) compared to that of freshwater fluxes (de Boer et al., 2007, 2008; Prange et al., 1997). Previous studies have shown that the reduced influence of freshwater tends to favor Pacific overturning (de Boer et al., 2007, 2008). The distribution of freshwater and its relative impact on overturning would, therefore, be different from today.

The area-averaged FWF north of 40°N (see methods) differs significantly between the models and ranges between 1.5 and 2.6 × 10^{-5} kg/m^2/s in the Atlantic and 1.5–3.5 × 10^{-5} kg/m^2/s in the Pacific. There is no negative correlation between the overturning in each basin and the local FWF (Figures 7a and 7b). The overturning strength in each basin is, therefore, substantially impacted by other external factors. However, the difference in overturning between these basins (i.e., AMOC-PMOC) is well correlated with the difference in FWF between these basins ($r = -0.76$, $p = 0.0016$, Figure 7c). Such a correlation is all the more meaningful when one considers the different model physics and boundary conditions in the different simulations. It appears that there is competition for overturning in the Northern Hemisphere, and the strongest convection occurs in the basin with the weakest surface FWF. This was also found to be the case for DeepMIP-Eocene simulations, where the regions with the least freshwater gain exhibited deepwater formation, especially in the Northern Hemisphere (Y. Zhang et al., 2022). This correlation between the difference in surface freshwater flux and the difference in overturning strength is not seen in the PI simulations (Figure S5 in Supporting Information S1), likely due to the absence of strong overturning in the Pacific in PI. It could also mean that surface freshwater flux had a larger control over the overturning basin in the Miocene than PI.

The surface FWF impacts the overturning by decreasing the salinity and, thus, the density of the upper layer. While the Miocene was warmer than today, the polar regions in these simulations are still quite cold in winter (Burls et al., 2021), and the nonlinearity of the equation of state of seawater implies that, at low temperatures, the variations in density are dominated by changes in salinity rather than temperature (de Boer et al., 2008; Prange et al., 1997). Indeed, there is a reasonable correlation between the AMOC strength and surface salinity in the Atlantic ($r = 0.68$, $p = 0.0074$, Figure 8a). As before, the correlation is impressive in light of the wide variety of physics and boundary conditions used in the simulations. There is no similar correlation in the Pacific, but perhaps this is not so surprising given that there are only three models with a PMOC strength greater than 2 Sv (Figure 8b).

We do find that the difference in overturning strength in the basins, that is, AMOC-PMOC, is correlated to the difference in salinity between the basins ($r = 0.63$, $p = 0.0148$, Figure 8c), though this correlation is somewhat weaker than the correlation of AMOC with Atlantic salinity (Figure 8a). The AMOC is better correlated to local salinity than local FWF (Figures 7a and 7b), because of the positive salinity feedback in which deep convection in the basin leads to increased salt import in that basin. Specifically, the basin salinity is not only set by surface FWF
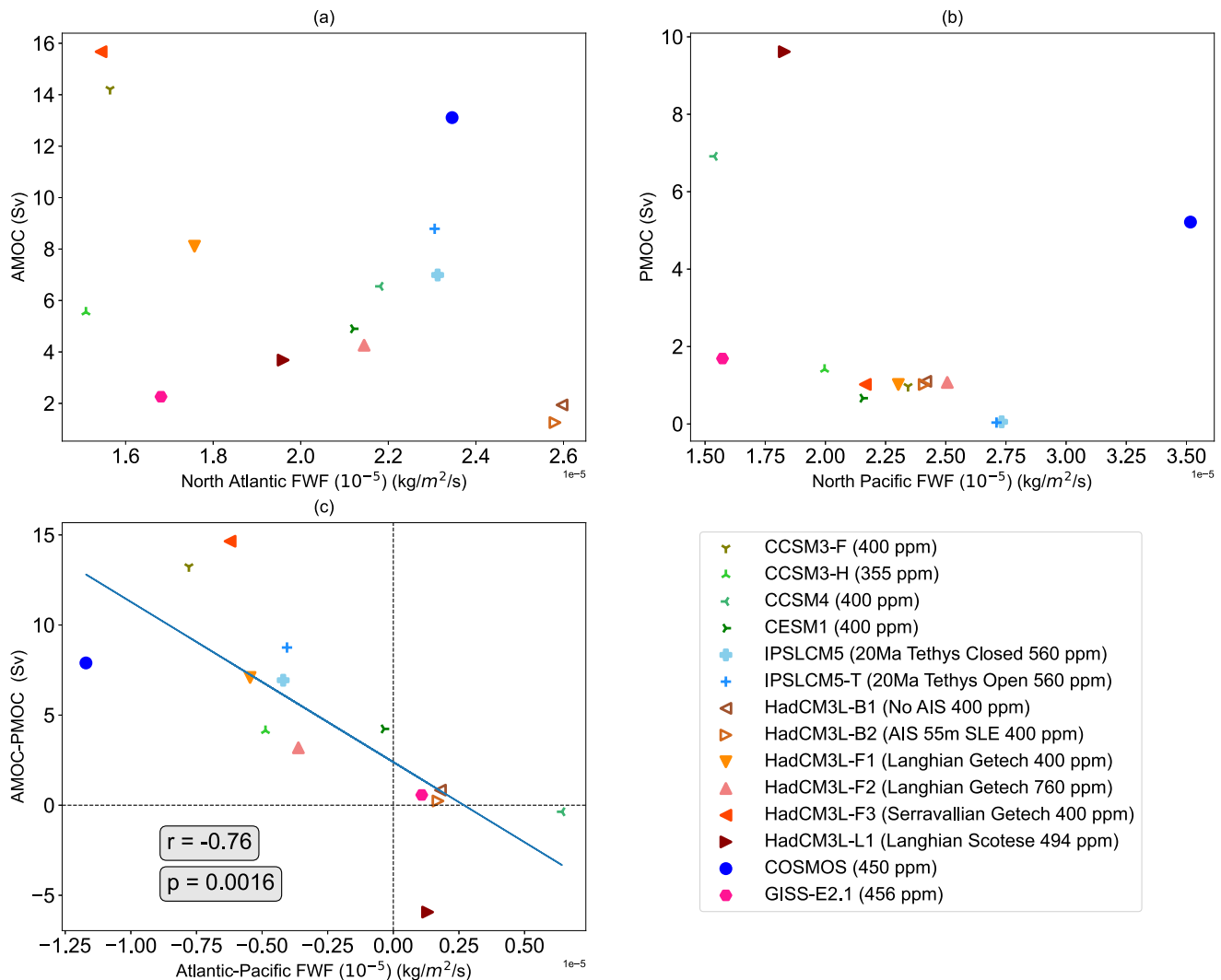
Figure 7. The strength of overturning in the basin versus the surface freshwater flux (FWF) received by the basin in (a) the North Atlantic and (b) the North Pacific in the Miocene simulations. (c) The difference in overturning between the North Atlantic and North Pacific versus the difference in FWF received by each. FWF = Precipitation-Evaporation + Runoff (above 40°N in both basins). The gray boxes indicate the Pearson correlation coefficient: $r = -0.76$ and the p-value: $p = 0.0016$.

but also influenced by advective freshwater transports at its horizontal boundaries, and these are themselves affected by the overturning and interbasin transport (Buckley & Marshall, 2016; Putrasahan et al., 2019). During the Miocene, interbasin transport was stronger than today due to the open tropical gateways. The salinity and FWF in the Atlantic and Pacific are negatively correlated, but there are a few outliers (~3, Figure S6 in Supporting Information S1).

Arguably, one of the most distinctive features across all our Miocene simulations is the fresh Arctic Ocean with mean surface salinity lower than 30 g/kg (Figure S7 and Table S4 in Supporting Information S1). This fresh Arctic Ocean is partly maintained by the net positive surface freshwater flux received by the basin, which is higher in the Miocene than PI (Table S4 in Supporting Information S1). The other reason for a fresher Arctic Ocean is that it was largely isolated from the rest of the world's oceans throughout much of the Cenozoic. It was sealed on the Pacific side by the emergent Beringia isthmus (i.e., no Bering Strait), and before the Miocene, there was no deepwater connection to the rest of the world's oceans, even on the Atlantic side (Kristoffersen, 1990; O'Regan et al., 2011; Waddell & Moore, 2008). The opening of the Fram Strait for deep water exchange during the Miocene (~17.5 Ma) connected it to the rest of the world's oceans (Jakobsson et al., 2007). Warmer temperatures during the Cenozoic meant stronger hydrological cycles, increased atmospheric poleward moisture transport, and thus an increase in
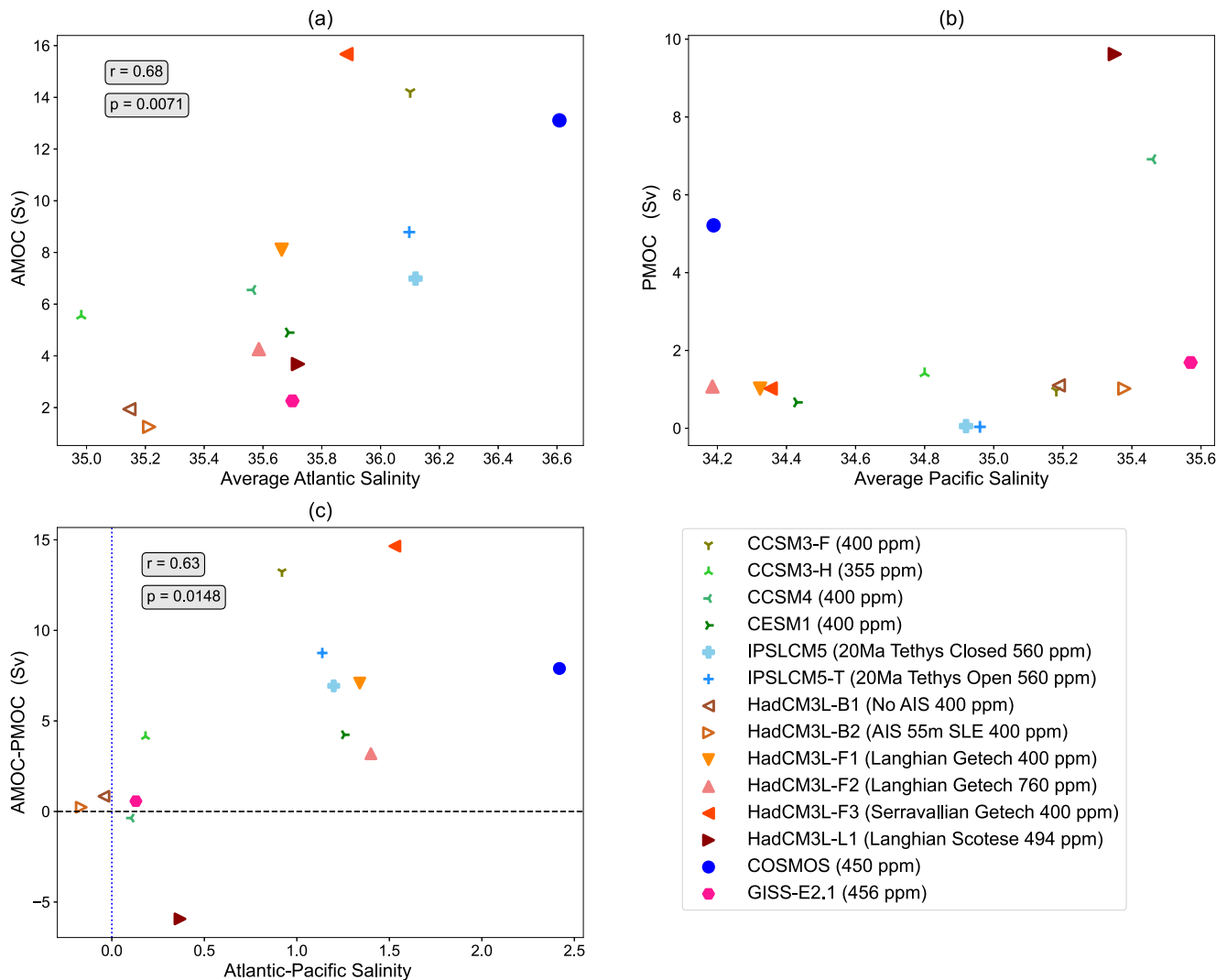
Figure 8. The strength of overturning versus the upper layer basin salinities in (a) the North Atlantic and (b) the North Pacific. The salinity is the volume-weighted average salinity in the respective basin above 500 m and north of 10°N. The gray boxes in panel (a) indicate the Pearson correlation, $r = 0.68$, and the p-value, $p = 0.0074$. (c) Difference in AMOC and PMOC versus the difference in North Atlantic and North Pacific salinity ($r = 0.63$, $p = 0.148$).

river runoff (Acosta et al., 2024; Cramwinckel et al., 2023). This, along with the absence of a substantial connection to the other oceans, meant that the Arctic was fresher than today before and throughout most of the Miocene (Brinkhuis et al., 2006; Sangiorgi et al., 2008). This remarkably fresh Arctic results in a high liquid freshwater flux through the Fram Strait compared to modern values; but, there is no correlation between this freshwater transport and the strength of the AMOC across the simulations (Figure 9). However, the majority of the simulations have a higher Arctic FWT than today (modern liquid FWT ~0.18 Sv; H. Wang et al., 2018) as well as a much weaker AMOC, suggesting that the general background state of fresh Arctic salinity found in all simulations (Figure S7 and Table S4 in Supporting Information S1) may contribute to the generally weaker AMOC.

It should be noted that we have not considered sea ice flux through the Fram Strait here, which is known to have a considerable impact on the deep water formation in the North Atlantic today (Ionita et al., 2016).

4.2. Impact of Orography

The presence of mountain ranges has been proposed to considerably impact the ocean circulation and location of deep-water formation regions on the planet by modifying atmospheric freshwater transport (e.g., Jiang & Yang, 2021; Yang et al., 2024). In climate model simulations with a completely flat orography, the meridional
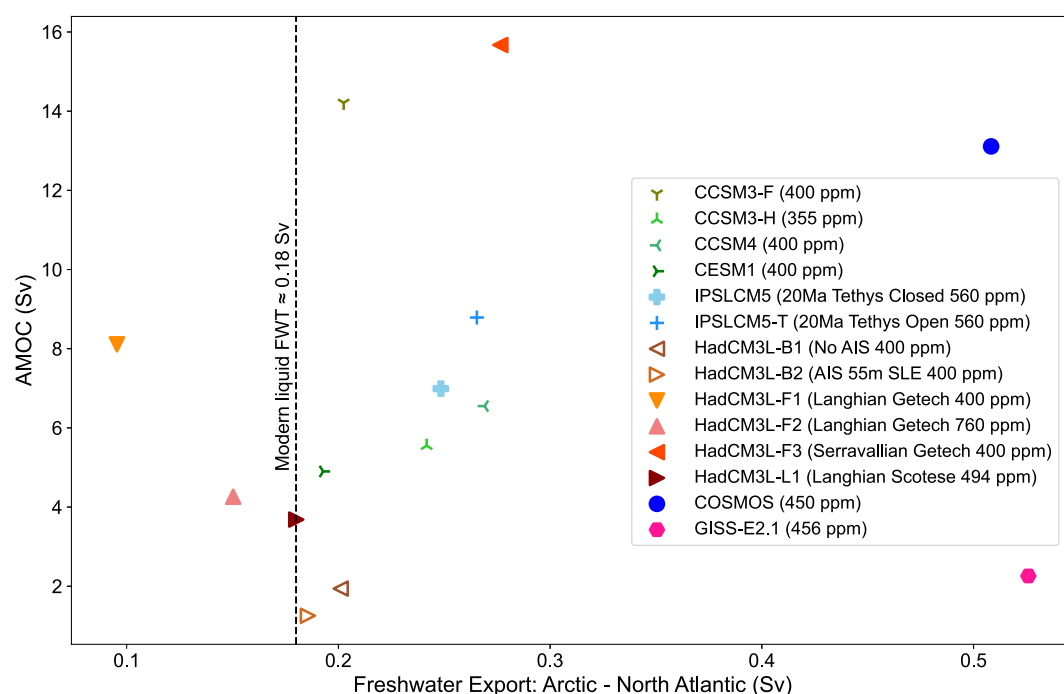
Figure 9. The strength of AMOC (Sv) versus the liquid freshwater export (Sv) from the Arctic to the North Atlantic in the Miocene simulations. The dashed line indicates modern liquid freshwater export from the Fram Strait (~0.18 Sv; H. Wang et al. (2018)). The freshwater export is calculated as per Section 2.3.

overturning switches from a North Atlantic-dominated circulation to one that is dominated by North Pacific deep-water formation (Maffre et al., 2018; Sinha et al., 2012). Some of the orographic features that have specifically been identified to significantly reshape the global deep water formation patterns are the Tibetan Plateau and the Rocky Mountains. The timing of the Tibetan Plateau uplift has been highly debated, but in recent years, studies have suggested that the uplift was asynchronous across the region and is believed to have started with the India-Asia collision during the Eocene with the completion of the uplift in the Miocene (~15-8 Ma) (Ding et al., 2022; C. Wang et al., 2014). This uplift is said to have changed the deep-water formation sites in the Northern Hemisphere from the North Pacific to the North Atlantic by reorganizing surface pressure patterns and freshwater fluxes and, consequently, the vertical mixing in the ocean (Su et al., 2018; Wen & Yang, 2020). The Rocky Mountains formed before the Miocene (Fan et al., 2014; Sjostrom et al., 2006). They may have stood higher than present before the Miocene and lowered during the middle Miocene (Chamberlain et al., 2012; Wolfe et al., 1997). Note that, here, we mean the entire North American Cordillera when we refer to the Rocky Mountains since the models do not have high enough resolution to resolve the details of the smaller mountain ranges within the Cordillera. Some theories for current NADW formation suggest that the Rocky Mountains block the atmospheric transport of freshwater from the Pacific and Indian oceans into the North Atlantic and thus help maintain the higher salinity in the Atlantic, favoring an AMOC instead of PMOC (Maffre et al., 2018; Sinha et al., 2012). However, other model sensitivity experiments have found a negligible impact of the Rocky Mountains on AMOC or PMOC strength (Jiang & Yang, 2021; Yang et al., 2024).

The early and middle Miocene simulations used in this study have vastly different reconstructions of the height and size of the Rocky Mountains and Tibetan Plateau (Figure 1), and thus, here, we can test the theories of the impact of orography on ocean circulation mentioned above. However, the previous model simulations that test the impact of orography tend to flatten the orography completely, global or regional (Maffre et al., 2018; Sinha et al., 2012; Su et al., 2018), while our simulations only have relatively smaller differences in the height of Tibetan Plateau or Rocky Mountains (Figure 1). This means that the impact of orography observed in other studies would be more noticeable than in our study.

Neither the Rocky Mountains nor the Tibetan Plateau shows any obvious correlation to AMOC and PMOC across the simulations (Figure 10). When looking at the group simulations carried out with the same model from the
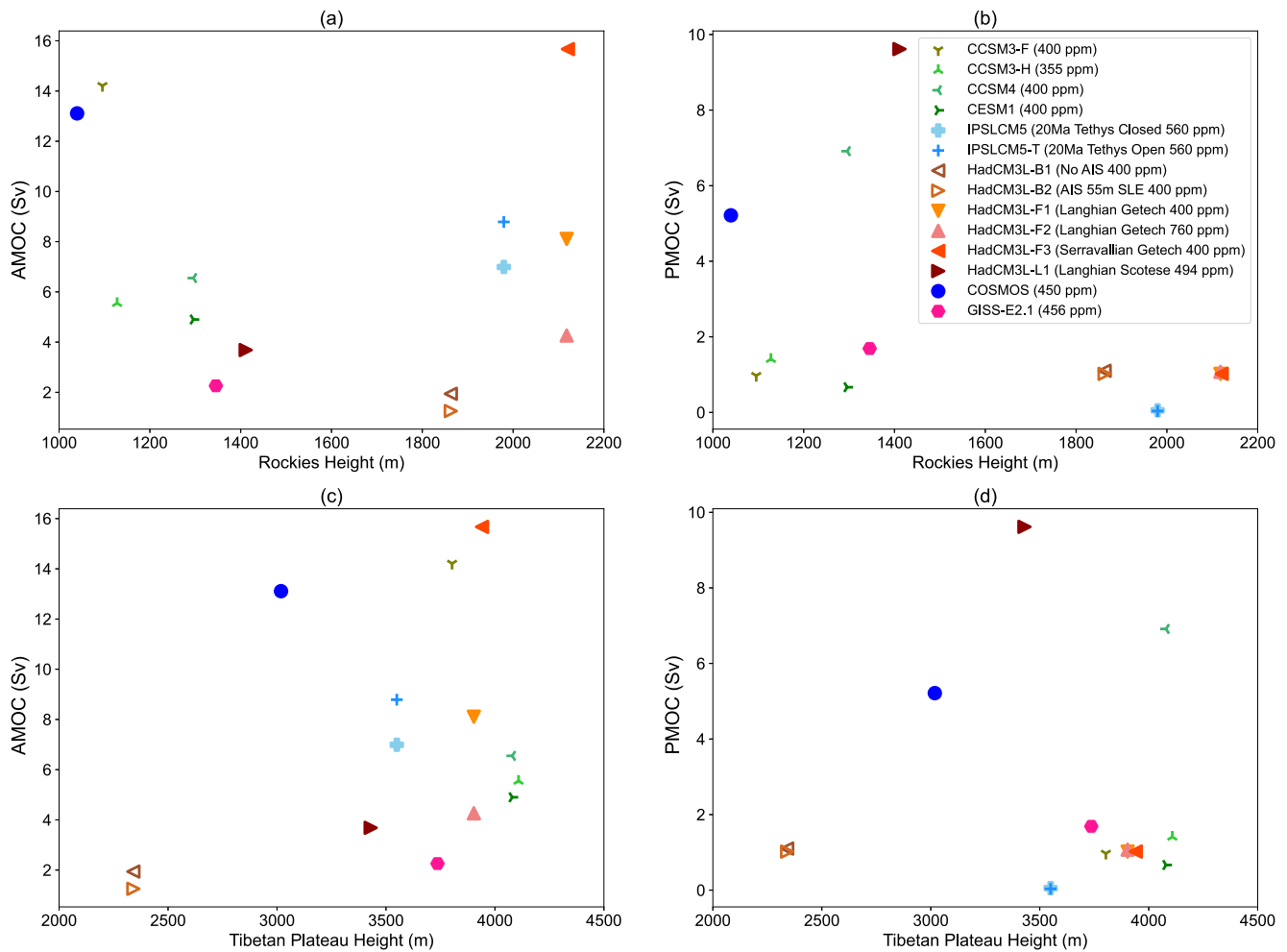
Figure 10. The impact of orographic height on overturning strength. (a) AMOC versus Rocky Mountains height, (b) Pacific Meridional Overturning Circulation (PMOC) versus Rocky Mountains height, (c) AMOC versus Tibetan Plateau height, (d) PMOC versus Tibetan Plateau height. The height of both is calculated as the mean height above a certain elevation cut-off, which is 800 m for the Rocky Mountains and 2,000 m for the Tibetan Plateau.

Hadley Centre (Figure 10a, orange/red triangles) we see that the only model that has a PMOC, HadCM3L_L1, has a lower Tibetan Plateau and Rocky Mountains comparatively. HadCM3L_L1 also has a more southern extent of the Tibetan Plateau and a reduced extent of the Rocky Mountains compared to the other in the model family (Figure 1). It has been shown that as the Tibetan Plateau migrated northwards, there was an increase in precipitation over the northwestern Pacific Ocean (C. Zhu et al., 2019). This could be part of the reason that HadCM3L_L1 has a lower surface freshwater flux in the Pacific compared to the other HadCM simulations (Figure 7b), which have helped in establishing a PMOC. A PMOC is present in only those simulations with a lower height of the Rocky Mountains (<1,500 m: Figure 10b). This is in agreement with the theory that with lower Rocky Mountains, there is excess moisture supply to the North Atlantic, and the North Pacific freshwater flux is reduced. Thus, a PMOC is possible. However, given that this result is from just one model and that the difference in mountain ranges is not the only difference between these simulations, this result should be treated with caution.

4.3. Impact of Strait Transports

The closing of tropical gateways during the Miocene restricted volume and freshwater transport between the Atlantic, Indian, and Pacific Oceans. Here, we investigate the impact of the strait volume transport (VT) on the overturning. An Nd isotope record of intermediate waters in the Florida Straits over the past 12.5 million years suggests that the restriction of Panama Seaway led to a stronger AMOC (Karas et al., 2017; Kirillova et al., 2019;
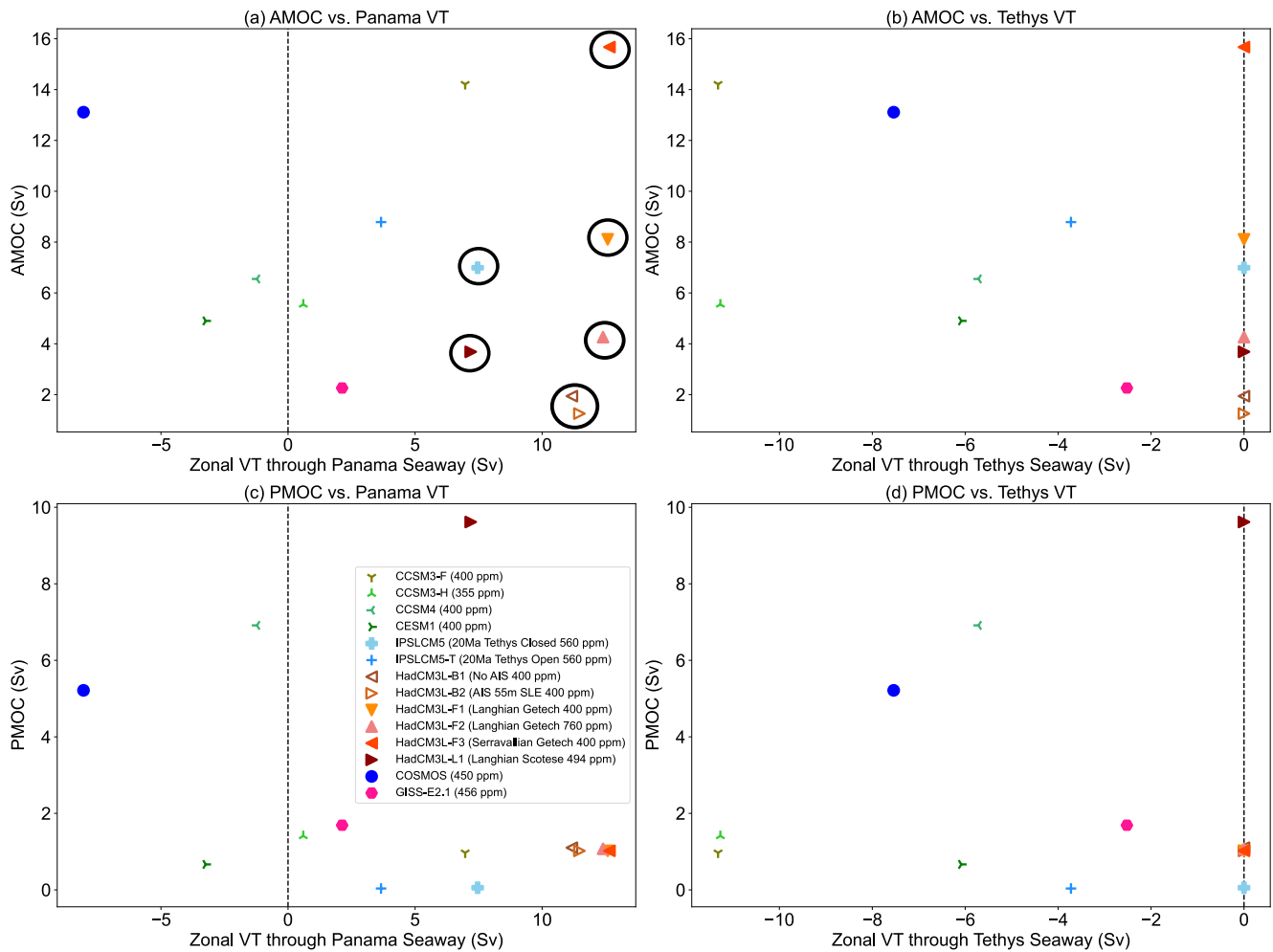
Figure 11. The relationship between the volume transport and the overturning strength. The *Y*-axis shows the maximum overturning streamfunction, which is defined as described in the methods. (a) AMOC versus VT through Panama Seaway, (b) AMOC versus VT through Tethys Seaway, (c) Pacific Meridional Overturning Circulation (PMOC) versus VT through Panama Seaway, and (d) PMOC versus VT through Tethys Seaway. The dashed lines in panels (a and c) separate the flow into positive (Pacific to Atlantic) and negative (Atlantic to Pacific). The VT through Tethys Seaway is always westward (negative). Simulations with a closed Tethys Seaway are placed at $x = 0$ in panels (b and d), denoting zero Tethys VT.

Osborne et al., 2014). So far, the modeling evidence for the impact of the Panama Seaway on the AMOC is ambiguous (Brierley & Fedorov, 2016; Butzin et al., 2011; Krapp & Jungclaus, 2011; Lunt et al., 2008).

Here, we find that neither Panama nor the Tethys volume transport correlates to the strength of the AMOC (Figures 11a and 11b). However, all the simulations with closed Tethys have an eastward flow through the Panama Seaway (Figure 11a, circled). Those with open Tethys that have a relatively strong (>1 Sv) eastward flow through Panama have an AMOC above 6 Sv (Figure 11a, squares). The VT through these seaways does not correlate to the PMOC strength. Interestingly, the PMOC is only present in simulations with a Panama Seaway deeper than 2,500 m (Figure S8 in Supporting Information S1).

5. Insights From Proxy Data

A multitude of approaches and proxies are available to provide insight into ocean circulation throughout the deep and recent past. These include geochemical, sedimentological, and micropaleontological proxies on a range of scales. Although proxy records may not allow for a direct comparison of overturning strength between today and the Miocene, they can reveal relative changes in overturning strength within the Miocene. Here, we summarize three key proxies to gain an understanding of the evolution of overturning throughout the Miocene.

5.1. Sediment Drift Deposits

A key sedimentological approach is to recognize and map large-scale seafloor sedimentary deposits known as sediment drifts or contourites (Stow & Smillie, 2020; Stow et al., 2002). Drift deposits are elongated mounds of seafloor sediments formed as a result of deposition by the deep oceanic boundary currents as their velocity varies as they "contour" around continental margins or other bathymetric obstacles. This sediment drift—deep current connection is especially apparent in the North Atlantic (Miller & Tucholke, 1983; Rebesco et al., 2014). The structure and age of these drifts can be constrained using seismic reflection data and deep sediment cores from the International Ocean Drilling Program (IODP) sites in the North Atlantic (Müller-Michaelis et al., 2013). Some of the earliest evidence for the drift formation and this initiation of deep circulation in the North Atlantic appears to be in the Eocene and the Oligocene, with a change in the style of drift deposition possibly due to an intensification of deep current circulation in the middle/late Miocene (Boyle et al., 2017; Miller & Tucholke, 1983). Other studies find increased drift formation in the early Miocene, suggesting a more vigorous flow of the undercurrent, likely due to the deepening of the Greenland Scotland Ridge, which allowed cold, deep Arctic and subpolar North Atlantic waters to flow southwards (Müller-Michaelis et al., 2013; Uenzelmann-Neben & Gruetzner, 2018). Several drifts grew significantly during the middle Miocene, suggesting a stronger effect of the undercurrent on deep sedimentation and thus, by inference, strengthened deep-water formation in the North Atlantic (Müller-Michaelis & Uenzelmann-Neben, 2014). A limitation of this approach is that the currents shaping the sedimentary drifts do not necessarily have to originate from deep water formation in the North Atlantic and can be influenced by water masses originating from other regions, such as the Southern Ocean or even the Indian and Pacific Oceans (Rebesco et al., 2014), either of which could have been important with Miocene gateway configurations.

5.2. Neodymium Isotopes

Another common proxy for ocean circulation is Neodymium (Nd) isotopic ratios (εNd), which is defined as ^{143}Nd/^{144}Nd normalized to the bulk Earth value and is used as a water mass provenance and mixing tracer. Nd has a short residence time in seawater, in the range of 200–2000 years (Jeandel et al., 1995; Tachikawa et al., 1999), and it is sourced mainly from terrigenous weathering inputs. Different ocean basins and, thus, deep ocean currents have distinct Nd isotopic compositions due to the specific Nd isotope contributions from surrounding land masses. Sediments deposited under the influence of these different deep-water currents carry the associated εNd signature into the geological records, to be extracted either by analysis of bulk sediments or fish teeth and fish skeletal debris, which develop Nd-rich diagenetic coatings at the seafloor (Martin & Scher, 2004). By measuring variability in εNd in these materials from sediment core samples from the North Atlantic region, it should be possible to infer variability in water masses over time. Using this proxy, the history of the deep-water formation in the North Atlantic, North Pacific, and Southern Ocean is explored here.

In the Atlantic, the Nd isotopic record points toward the initiation of NCW formation in the Nordic Seas in the early Oligocene (∼33 Ma) due to the deepening of the Greenland-Scotland Ridge, with an increasing export of NCW to the Southern Ocean toward the late Oligocene (Scher & Martin, 2008; Via & Thomas, 2006). The possible onset of deep convection in the Labrador Sea is recorded in εNd data from the South Atlantic during the late Miocene, between ∼10 and 7 Ma, although part of the signal could be attributed to an increased input of non-radiogenic Nd due to a change in mechanical weathering (Thomas & Via, 2007).

Using the εNd approach, the study of multiple sites across the Pacific suggests that the Pacific might have had bipolar overturning until about 40 Ma, after which the formation of North Pacific Deep Water (NPDW), producing a PMOC, slowed down. The circulation pattern is thought to have gradually changed to the modern-like diffusive formation of the Pacific Deep Water (PDW) by about 25 Ma (McKinley et al., 2019), or as late as ∼14 Ma, after which a southern source (Circumpolar Deep Water (CDW)) is detected in the Northwest Pacific (Kender et al., 2018).

Evidence of Southern Ocean deepwater formation in the South Pacific can be found using εNd data from multiple deep-sea sediment cores from the early Paleocene (Thomas et al., 2014). In the Oligocene, εNd values in the Kerguelen Plateau region do not show a large change but a gradual shift toward less radiogenic values suggestive of a strengthening of the proto-CDW enhanced export and entrainment of the NCW into the Southern Ocean (N. M. Wright et al., 2018). Thus, there is evidence for the Southern Ocean overturning long before the Miocene. In the Miocene, the Pacific overturning circulation might have started to resemble modern patterns, with a sluggish northern cell and a relatively stronger and deeper southern cell. This has been linked to the mid-Miocene Climatic

Transition (MMCT), ~14 Ma, coincident with the expansion of the Antarctic ice sheet (Kender et al., 2018). In summary, the deep-water formation in the Southern Ocean had been present since at least the Eocene and continued throughout the Miocene (Y. Zhang et al., 2022). Drawbacks of Nd isotopes reconstructions, including, among other things, the complexity of Nd sources, as well as overlapping ϵNd values between different water masses which can pose challenges in accurately tracing water mass provenance and reconstructing basin-wide circulation changes (McKinley et al., 2019).

5.3. Carbon Isotopes (δ^{13}C)

The carbon isotope ratio δ^{13}C (expressed as ratios of ^{13}C/^{12}C of the sample compared to the isotope ratio of a known standard), derived from benthic foraminifera fossil shells from sediment cores, is used to infer changes in past ocean circulation patterns (Miller et al., 1987; Woodruff & Savin, 1989). The comparison of values of δ^{13}C from the different oceanic basins helps in determining the age/ventilation of the water masses above the sites and, thus, the different pathways for deep circulation. In the modern ocean, photosynthesis in the surface ocean preferentially consumes the lighter ^{12}C, and thus, the surface ocean is enriched in ^{13}C (high δ^{13}C$_{DIC}$ values), while the low δ^{13}C carbon is exported to the deep ocean in the form of particulate organic matter which then leads to low δ^{13}C$_{DIC}$ values in the deep ocean (Ravelo & Hillaire-Marcel, 2007). When deep water forms in the high North Atlantic latitudes, it acquires its signature of relatively high δ^{13}C from well-ventilated, ^{12}C-depleted surface water masses exported from lower latitudes. As the water mass ages, ^{12}C is returned through bacterial decomposition, and its δ^{13}C$_{DIC}$ value decreases the longer it remains out of contact with the surface. In contrast, the modern North Atlantic, with a strong AMOC, NADW is enriched in δ^{13}C$_{DIC}$ while the deep North Pacific, with no current deepwater production, is depleted in δ^{13}C$_{DIC}$ due to a continuous input of organic carbon (Kroopnick, 1985). In the case of the Miocene, interpreting the time series of benthic foraminifera δ^{13}C, Woodruff and Savin (1989) concluded that there was no deep-water formation in the North Atlantic before 14.5 Ma, with the deep waters being depleted in δ^{13}C and the water mass aged from south to north, and suggesting that the deepest waters in the Atlantic predominantly formed in the Southern Ocean. Between 14 and 11 Ma, the NCW formation was weak and might have grown to modern strength after 11 Ma (Woodruff & Savin, 1989). Increasing the resolution of the benthic δ^{13}C records, J. D. Wright et al. (1992), found that the North Atlantic had episodes of high δ^{13}C values from 19 to 16 Ma, implying pulses of NCW production at this time. Poore et al. (2006) found strong evidence of overflow of NCW over the GSR after 12 Ma, and this overflow changed with the vertical motions of the GSR, as discerned by the changing δ^{13}C values in the Southern Ocean. Global δ^{13}C compilations revealed two significant events in the Miocene δ^{13}C record. First, the δ^{13}C values of the North Atlantic and North Pacific diverged in the middle Miocene between ~13 and 10 Ma, likely due to the initiation of GSR overflow due to the deepening of the GSR and, thus, an increase in NCW production (Cramer et al., 2009; J. D. Wright & Miller, 1996). Subsequently, in the late Miocene (~7 Ma), δ^{13}C from the North and South Atlantic/Subantarctic Oceans diverged. This is explained by Atlantic-Pacific basin isolation as a result of the shoaling of Panama Seaway, causing an increase in North Atlantic salinity and a cooling of the ocean below ~4°C leading to a haline overturning, thereby strengthening the NCW production and causing an export further south (Cramer et al., 2009; Lear et al., 2000).

In summary, these multiple proxies paint a complicated picture of the history of deep water formation, especially in the North Atlantic. Initiation of the deep water formation in the North Atlantic likely occurred sometime in the Oligocene, maybe as early as the Eocene, and it intensified in the Miocene, the exact timing of which is debated. Some evidence for Miocene deep water formation in the North Pacific is found, and it stopped around 40 Ma, 25 Ma, or 14 Ma, according to different interpretations, while the Southern Ocean has been a prominent source and deep and bottom waters throughout the Cenozoic.

6. Age Ranges of the Miocene Simulations

Here, we investigate potential inconsistencies between the targeted age (or age range) for the Miocene simulations and the ages we have assigned using the paleogeographic features, which may provide a more accurate estimate of the time range they represent. To accomplish this, we assign a date or a date range to each simulation (see Section 2.4). The paleogeographies used here are designed to represent a specific time or time range, and this is provided in the associated publications. We refer to this as the simulation's "target age." We then use both our paleogeographic ages and the target ages to investigate the differences between the two (Figure 12).
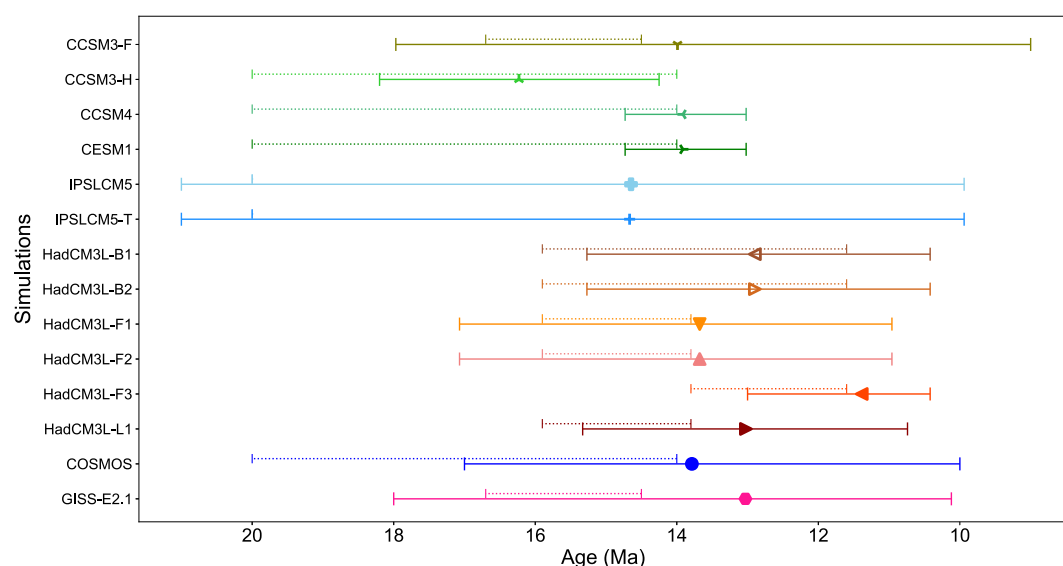
Figure 12. The estimated paleogeographic ages of the Miocene simulations, which were calculated for the Panama Seaway, Tethys Seaway, and the Fram Strait using the method described in Section 2.4. The solid bars are the ages we estimate, and the bars with the dotted line just above each solid bar with the same color are the target ages that the simulations were initially run with. The symbols on the solid bars are placed at the mean age calculated from the three straits, with the endpoints being the maximum and minimum ages we estimate.

It is difficult to place some simulations according to the straits as they were specifically run for experiments about the effect of gateway changes on ocean circulation. For example, IPSLCM5 and IPSLCM5T were run with the paleogeography for 20 Ma but with experiments on testing the effect of an open versus closed Tethys Seaway (Pillot et al., 2022). With other simulations using different paleogeographies that had a deeper Tethys Seaway, IPSLCM5 and IPSLCM5T were placed at ~13 Ma, while a very shallow Fram Strait placed them at 21 Ma. This resulted in a very wide range of possible ages for these two simulations. The use of different paleogeographies, and thus having different strait geometries and the resolution of each simulation, also has an effect on the strait areas. This made it difficult to quantitively calculate the areas of straits in the different simulations and subsequently place them on the timeline. There remains a large uncertainty in the width and depth of straits that are crucial for ocean circulation, resulting in such a large spread in paleogeographies across the Miocene simulations, even when the same time period is targeted. This highlights the need for a more careful selection of paleogeography and that more investigation is necessary to constrain events like opening and closing of gateways to narrow the possible age ranges.

7. Discussion and Conclusions

The ocean circulation in the simulations exhibits large variability in every aspect, from the overturning to the exchanges between basins. These differences are model-dependent but also arise due to the difference in paleogeographies used. The simulations from the same model family have different model physics between the different versions, which would impact the overturning circulation. For example, different cloud physics impacts the radiative balance and precipitation, while different diapycnal diffusivity parameterizations would impact the diffusive overturning. Given the wide array of model differences, we cannot isolate the impact of particular model parameterizations in this uncontrolled study. In general, the Southern Ocean overturning dominates more over the Northern Hemisphere overturning during the Miocene than today. This is not because the SOMOC was stronger but because the Northern Hemisphere overturning, and primarily the AMOC, was weaker. The local overturning in the southern cell is stronger in the Miocene compared to PI, but this does not lead to a stronger bottom cell (SOMOC in this study), which is diffusively driven. This suggests that the various model physical parameterizations that impact the SOMOC, such as diapycnal mixing, are more important than the changing boundary conditions such as Southern Ocean winds or buoyancy forcing (and emphasizes a need to better understand the controls on this cell). All the simulations have an AMOC that is weaker than in the pre-industrial simulations

(Figure S4 and Table S2 in Supporting Information S1) and also the modern observed value, which is ∼17 Sv (Frajka-Williams et al., 2019), with only 3 of 14 simulations having an AMOC stronger than 10 Sv. In the PI North Atlantic, the Nordic Seas have prominent deep MLDs in all simulations (Figure S2 in Supporting Information S1). However, in the Miocene simulations, only one simulation shows deep MLD in the Nordic Seas. This is likely because exchange with the Arctic Ocean was restricted, owing to the presence of the Barents Sea Landmass and a narrow connection between the Arctic and North Atlantic. This may have inhibited the cooling and densification of Atlantic water entering the Nordic Seas and Arctic Ocean, which is an important mechanism for deep water formation in the Nordic Seas today (Brakstad et al., 2023). Burls et al. (2021) showed that the North Atlantic exhibits a prominent cold bias in the Miocene compared to proxies, and we find weaker AMOC in our study. Some proxy records indicate an increased NCW production during warmer intervals (H. Wang et al., 2023). To address these discrepancies, future work could investigate AMOC behavior in higher CO_2 simulations of the Miocene to determine whether it strengthens, bringing the results more in line with proxy SSTs.

Unlike the modern day, there are 3 of 14 Miocene simulations with a PMOC, albeit weak (∼5–10 Sv). The set of simulations, including members with an AMOC and a PMOC, offers the chance to explore factors that impact the location of Northern Hemisphere deep water formation. We test some previous hypotheses that are directly or indirectly related to the choice of the Northern Hemisphere deep water formation basin. Those related to (a) surface FWF, (b) tropical straits, and (c) orography, and we discuss each in turn. We also briefly discuss the impact of Arctic freshwater export.

First, the modern dominance of overturning in the Atlantic has been attributed to the excess surface FWF in the Pacific compared to the Atlantic (Ferreira et al., 2018). Here, we find that the dominance of AMOC over PMOC is indeed correlated with the excess surface FWF of the Pacific compared to the Atlantic ($r = -0.76$, $p = 0.0016$). It is striking that a significant correlation is found across such a medley of models and boundary conditions, and this points to a robust control on overturning basin. A similar correlation is also found between the AMOC-PMOC and the differences in basin salinity, but this is weaker because the basin salinity is also controlled by horizontal freshwater transports that are themselves dependent on the overturning. Second, the intensification of the AMOC (possibly related to a weakening of the PMOC) has been associated with the shoaling of the Panama Seaway (Kirillova et al., 2019; Osborne et al., 2014). While there is no correlation between the volume transport through the Panama Seaway or the Tethys Seaway and the AMOC or PMOC across these simulations, we do find that simulations with a shallow Panama Seaway (<1,000 m) only have an AMOC, and all the simulations with a PMOC have a deep Panama Seaway (>2,500 m; Figure S8 in Supporting Information S1). Third, the rise of the Tibetan Plateau and the Rocky Mountains has been suggested to decrease the PMOC, potentially promoting an AMOC (Maffre et al., 2018; Wen & Yang, 2020). In this study, there is no obvious correlation between the height of the Rocky Mountains and Tibetan Plateau and the PMOC or between the orography and the difference between the PMOC and AMOC (Figure 10). Similar to the strait hypothesis, there is some support for this hypothesis, though. The simulations with a PMOC have the Rocky Mountains lower than 1,500 m and a low Tibetan Plateau. Fourth, a decrease in Arctic freshwater to the Atlantic has been indicated as a control for a strengthening AMOC at the expense of a PMOC (Hutchinson et al., 2019). In our study, there is no correlation across the simulations of the Arctic freshwater export to the Atlantic on the AMOC strength (Figure 9). This may be due to the strait geometry, feedback of ocean circulation on freshwater transports, and other external factors influencing AMOC strength, such as Atlantic FWF. Again, there is some support for the idea, though. The Miocene Arctic was much fresher than today (Table S4 and Figure S7 in Supporting Information S1), which stems from higher surface FWF in the Arctic Ocean in the Miocene compared to the PI (Table S4 in Supporting Information S1). Another reason for the fresher Arctic is that it was more isolated during the early and middle Miocene, restricting the mixing of freshwater with the wider ocean. Overall, most of the simulations have a freshwater export stronger than modern (modern liquid FWT ∼0.18 Sv; H. Wang et al., 2018), and the AMOC is weaker than PI in all the simulations.

The Southern Ocean deepwater formation is present in most of our simulations (Table S2 in Supporting Information S1), and the proxy evidence for a circulation controlled by the Southern Ocean sinking during the Miocene is quite strong. So, our simulations agree with the proxies that the Southern Ocean was likely the dominant source for deep and bottom waters throughout the Eocene and continued to be dominant in the Miocene. The proxy evidence for the existence of a PMOC during the Miocene is divided. While some sites suggest the possibility of a PMOC until ∼14 Ma (Kender et al., 2018), many others suggest a cessation of PMOC before the Miocene (McKinley et al., 2019; Thomas et al., 2014). By the Miocene, the AMOC had likely started to develop into its modern structure, and there could have been intermittent pulses of PMOC, which is supported by proxies (Kender

et al., 2018). Such a picture from proxy data agrees broadly with our results. We find an AMOC stronger in our simulation than during the Eocene (Y. Zhang et al., 2022) but weaker than today. Simulations with a PMOC have a deeper Panama Seaway and lower orography, features associated with the earlier Miocene, while simulations with a higher orography and shallower Panama Seaway, associated with later in the Miocene, are dominated by an AMOC. This suggests that if there were a PMOC in the Miocene, it was likely active in the early Miocene or late Oligocene.

In conclusion, the simulations reveal Miocene ocean circulation patterns that were remarkably different from today, owing to differences in paleogeographies and possibly, to some extent, the stronger greenhouse forcing. This study has many uncertainties but is the most comprehensive comparison so far about the role of different paleogeographies on ocean circulation. Previous hypotheses tested here of the impact of paleogeographic features on the overturning are not robust across this ensemble with its array of models and boundary conditions but find some support. A formal MIP would be useful to distinguish the impact of different models in simulating the overturning circulation during the Miocene. However, specific MIPs spanning the entire Miocene and testing uncertainties in the paleogeographic features are needed to make progress in our understanding of the evolution of the Miocene circulation and its sensitivity to straits and orography. In this study, we find evidence for the importance of the depth of Panama Seaway and the height of the Tibetan Plateau on the strength of overturning. Hence, sensitivity studies focusing on these factors could help untangle the importance of each of them on ocean circulation during the mid-Miocene. It would also be useful to extend this analysis to the late Miocene when the Panama Seaway was closed, as its importance then remains a heavily debated topic. Thus, an ambitious but important long-term goal would be to move toward model intercomparisons that sample the range of Miocene paleogeographies in time and uncertainty. The ongoing development of climate models to address current problems (e.g., with convection parameterization and capturing observed polar amplification), along with new proxy data, will lead to continuous improvement in our understanding of the Miocene ocean circulation.

Data Availability Statement

The data set used to create the figures in this manuscript is available at Naik et al. (2025). The Python code used to generate all figures is available at https://github.com/trushanaik/MioMIP1-Ocean-Intercomparison and archived at Naik (2025).

References

Abelson, M., & Erez, J. (2017). The onset of modern-like Atlantic meridional overturning circulation at the Eocene-Oligocene transition: Evidence, causes, and possible implications for global cooling. *Geochemistry, Geophysics, Geosystems*, *18*(6), 2177–2199. https://doi.org/10.1002/2017gc006826

Acosta, R. P., Burls, N. J., Pound, M. J., Bradshaw, C. D., De Boer, A. M., Herold, N., et al. (2024). A model-data comparison of the hydrological response to Miocene warmth: Leveraging the MioMIP1 opportunistic multi-model ensemble. *Paleoceanography and Paleoclimatology*, *39*(1), e2023PA004726. https://doi.org/10.1029/2023PA004726

Allen, M. B., & Armstrong, H. A. (2008). Arabia–Eurasia collision and the forcing of mid-Cenozoic global cooling. *Palaeogeography, Palaeoclimatology, Palaeoecology*, *265*(1–2), 52–58. https://doi.org/10.1016/j.palaeo.2008.04.021

Bialik, O. M., Frank, M., Betzler, C., Zammit, R., & Waldmann, N. D. (2019). Two-step closure of the Miocene Indian Ocean Gateway to the Mediterranean. *Scientific Reports*, *9*(1), 8842. https://doi.org/10.1038/s41598-019-45308-7

Borrelli, C., Cramer, B. S., & Katz, M. E. (2014). Bipolar Atlantic deepwater circulation in the middle-late Eocene: Effects of Southern Ocean gateway openings. *Paleoceanography*, *29*(4), 308–327. https://doi.org/10.1002/2012pa002444

Boyer, T. P., & Levitus, S. (2002). World ocean atlas 2001, *Salinity* (Vol. 2).

Boyle, P. R., Romans, B. W., Tucholke, B. E., Norris, R. D., Swift, S. A., & Sexton, P. F. (2017). Cenozoic North Atlantic deep circulation history recorded in contourite drifts, offshore Newfoundland, Canada. *Marine Geology*, *385*, 185–203. https://doi.org/10.1016/j.margeo.2016.12.014

Bradshaw, C. D., Langebroek, P. M., Lear, C. H., Lunt, D. J., Coxall, H. K., Sosdian, S. M., & de Boer, A. M. (2021). Hydrological impact of Middle Miocene Antarctic ice-free areas coupled to deep ocean temperatures. *Nature Geoscience*, *14*(6), 429–436. https://doi.org/10.1038/s41561-021-00745-w

Bradshaw, C. D., Lunt, D. J., Flecker, R., & Davies-Barnard, T. (2015). Disentangling the roles of late Miocene palaeogeography and vegetation – Implications for climate sensitivity. *Palaeogeography, Palaeoclimatology, Palaeoecology*, *417*, 17–34. https://doi.org/10.1016/j.palaeo.2014.10.003

Bradshaw, C. D., Lunt, D. J., Flecker, R., Salzmann, U., Pound, M. J., Haywood, A. M., & Eronen, J. T. (2012). The relative roles of CO_2 and palaeogeography in determining late Miocene climate: Results from a terrestrial model–data comparison. *Climate of the Past*, *8*(4), 1257–1285. https://doi.org/10.5194/cp-8-1257-2012

Brakstad, A., Gebbie, G., Våge, K., Jeansson, E., & Ólafsdóttir, S. R. (2023). Formation and pathways of dense water in the Nordic Seas based on a regional inversion. *Progress in Oceanography*, *212*, 102981. https://doi.org/10.1016/j.pocean.2023.102981

Brierley, C. M., & Fedorov, A. V. (2016). Comparing the impacts of Miocene–Pliocene changes in inter-ocean gateways on climate: Central American Seaway, Bering Strait, and Indonesia. *Earth and Planetary Science Letters*, *444*, 116–130. https://doi.org/10.1016/j.epsl.2016.03.010

Brinkhuis, H., Schouten, S., Collinson, M. E., Sluijs, A., Damsté, J. S. S., Dickens, G. R., et al. (2006). Episodic fresh surface waters in the Eocene Arctic Ocean. *Nature*, *441*(7093), 606–609. https://doi.org/10.1038/nature04692

Buckley, M. W., & Marshall, J. (2016). Observations, inferences, and mechanisms of the Atlantic Meridional Overturning Circulation: A review. *Reviews of Geophysics*, *54*(1), 5–63. https://doi.org/10.1002/2015RG000493

Burls, N. J., Bradshaw, C. D., De Boer, A. M., Herold, N., Huber, M., Pound, M., et al. (2021). Simulating Miocene warmth: Insights from an opportunistic multi-model ensemble (MioMIP1). *Paleoceanography and Paleoclimatology*, *36*(5), e2020PA004054. https://doi.org/10.1029/2020PA004054

Butzin, M., Lohmann, G., & Bickert, T. (2011). Miocene ocean circulation inferred from marine carbon cycle modeling combined with benthic isotope records. *Paleoceanography*, *26*(1), PA1203. https://doi.org/10.1029/2009PA001901

Chamberlain, C. P., Mix, H. T., Mulch, A., Hren, M. T., Kent-Corson, M. L., Davis, S. J., et al. (2012). The Cenozoic climatic and topographic evolution of the western North American Cordillera.

Cramer, B. S., Toggweiler, J. R., Wright, J. D., Katz, M. E., & Miller, K. G. (2009). Ocean overturning since the Late Cretaceous: Inferences from a new benthic foraminiferal isotope compilation. *Paleoceanography*, *24*(4), PA4216. https://doi.org/10.1029/2008PA001683

Cramwinckel, M. J., Burls, N. J., Fahad, A. A., Knapp, S., West, C. K., Reichgelt, T., et al. (2023). Global and zonal-mean hydrological response to early Eocene warmth. *Paleoceanography and Paleoclimatology*, *38*(6), e2022PA004542. https://doi.org/10.1029/2022PA004542

Crichton, K. A., Ridgwell, A., Lunt, D. J., Farnsworth, A., & Pearson, P. N. (2021). Data-constrained assessment of ocean circulation changes since the middle Miocene in an Earth system model. *Climate of the Past*, *17*(5), 2223–2254. https://doi.org/10.5194/cp-17-2223-2021

De Boer, A. M., & Hogg, A. M. (2014). Control of the glacial carbon budget by topographically induced mixing. *Geophysical Research Letters*, *41*(12), 4277–4284. https://doi.org/10.1002/2014gl059963

de Boer, A. M., Hutchinson, D. K., Roquet, F., Sime, L. C., Burls, N. J., & Heuzé, C. (2022). The impact of southern ocean topographic barriers on the ocean circulation and the overlying atmosphere. *Journal of Climate*, *35*(18), 5805–5821. https://doi.org/10.1175/jcli-d-21-0896.1

de Boer, A. M., & Nof, D. (2004a). The Bering Strait's grip on the northern hemisphere climate. *Deep Sea Research Part I: Oceanographic Research Papers*, *51*(10), 1347–1366. https://doi.org/10.1016/j.dsr.2004.05.003

de Boer, A. M., & Nof, D. (2004b). The exhaust valve of the North Atlantic. *Journal of Climate*, *17*(3), 417–422. https://doi.org/10.1175/1520-0442(2004)017<0417:TEVOTN>2.0.CO;2

de Boer, A. M., Sigman, D. M., Toggweiler, J. R., & Russell, J. L. (2007). Effect of global ocean temperature change on deep ocean ventilation. *Paleoceanography*, *22*(2). https://doi.org/10.1029/2005PA001242

de Boer, A. M., Toggweiler, J. R., & Sigman, D. M. (2008). Atlantic dominance of the meridional overturning circulation. *Journal of Physical Oceanography*, *38*(2), 435–450. https://doi.org/10.1175/2007JPO3731.1

Ding, L., Kapp, P., Cai, F., Garzione, C. N., Xiong, Z., Wang, H., & Wang, C. (2022). Timing and mechanisms of Tibetan Plateau uplift. *Nature Reviews Earth & Environment*, *3*(10), 652–667. https://doi.org/10.1038/s43017-022-00318-4

Ehlers, B. M., & Jokat, W. (2013). Paleo-bathymetry of the northern North Atlantic and consequences for the opening of the Fram Strait. *Marine Geophysical Researches*, *34*(1), 25–43. https://doi.org/10.1007/s11001-013-9165-9

Fan, M., Heller, P., Allen, S. D., & Hough, B. G. (2014). Middle Cenozoic uplift and concomitant drying in the central Rocky Mountains and adjacent Great Plains. *Geology*, *42*(6), 547–550. https://doi.org/10.1130/g35444.1

Farnsworth, A., Lunt, D. J., O'Brien, C. L., Foster, G. L., Inglis, G. N., Markwick, P., et al. (2019). Climate sensitivity on geological timescales controlled by nonlinear feedbacks and ocean circulation. *Geophysical Research Letters*, *46*(16), 9880–9889. https://doi.org/10.1029/2019GL083574

Feakins, S. J., Warny, S., & Lee, J.-E. (2012). Hydrologic cycling over Antarctica during the middle Miocene warming. *Nature Geoscience*, *5*(8), 557–560. https://doi.org/10.1038/ngeo1498

Ferreira, D., Cessi, P., Coxall, H. K., De Boer, A., Dijkstra, H. A., Drijfhout, S. S., et al. (2018). Atlantic-Pacific asymmetry in deep-water formation. *Annual Review of Earth and Planetary Sciences*, *46*(1), 1–26. https://doi.org/10.1146/annurev-earth-082517-010045

Frajka-Williams, E., Ansorge, I. J., Baehr, J., Bryden, H. L., Chidichimo, M. P., Cunningham, S. A., et al. (2019). Atlantic meridional overturning circulation: Observed transport and variability. *Frontiers in Marine Science*, *6*, 260. https://doi.org/10.3389/fmars.2019.00260

Frigola, A., Prange, M., & Schulz, M. (2018). Boundary conditions for the Middle Miocene Climate Transition (MMCT v1.0). *Geoscientific Model Development*, *11*(4), 1607–1626. https://doi.org/10.5194/gmd-11-1607-2018

Frigola, A., Prange, M., & Schulz, M. (2021). A dynamic ocean driven by changes in CO$_2$ and Antarctic ice-sheet in the middle Miocene. *Palaeogeography, Palaeoclimatology, Palaeoecology*, *579*, 110591. https://doi.org/10.1016/j.palaeo.2021.110591

Fyke, J. G., D'Orgeville, M., & Weaver, A. J. (2015). Drake Passage and Central American Seaway controls on the distribution of the oceanic carbon reservoir. *Global and Planetary Change*, *128*, 72–82. https://doi.org/10.1016/j.gloplacha.2015.02.011

Goldner, A., Herold, N., & Huber, M. (2014). The challenge of simulating the warmth of the mid-Miocene climatic optimum in CESM1. *Climate of the Past*, *10*(2), 523–536. https://doi.org/10.5194/cp-10-523-2014

Hamon, N., Sepulchre, P., Lefebvre, V., & Ramstein, G. (2013). The role of eastern Tethys seaway closure in the Middle Miocene Climatic Transition (ca. 14 Ma). *Climate of the Past*, *9*(6), 2687–2702. https://doi.org/10.5194/cp-9-2687-2013

Herold, N., Huber, M., & Müller, R. D. (2011). Modeling the Miocene climatic optimum. Part I: Land and atmosphere. *Journal of Climate*, *24*(24), 6353–6372. https://doi.org/10.1175/2011JCLI4035.1

Herold, N., Seton, M., Müller, R., You, Y., & Huber, M. (2008). Middle Miocene tectonic boundary conditions for use in climate models. *Geochemistry, Geophysics, Geosystems*, *9*(10), Q10009. https://doi.org/10.1029/2008GC002046

Heuzé, C. (2020). Antarctic bottom water and North Atlantic deep water in CMIP6 models. *Ocean Science Discussions*, *2020*, 1–38.

Hossain, A., Knorr, G., Jokat, W., & Lohmann, G. (2021). Opening of the Fram Strait led to the establishment of a modern-like three-layer stratification in the Arctic Ocean during the Miocene. *Arktos*, *7*(1–3), 1–12. https://doi.org/10.1007/s41063-020-00079-8

Hossain, A., Knorr, G., Lohmann, G., Stärz, M., & Jokat, W. (2020). Simulated thermohaline fingerprints in response to different Greenland-Scotland Ridge and Fram Strait subsidence histories. *Paleoceanography and Paleoclimatology*, *35*(7), e2019PA003842. https://doi.org/10.1029/2019PA003842

Huang, X., Stärz, M., Gohl, K., Knorr, G., & Lohmann, G. (2017). Impact of Weddell Sea shelf progradation on Antarctic bottom water formation during the Miocene. *Paleoceanography*, *32*(3), 304–317. https://doi.org/10.1002/2016PA002987

Hutchinson, D. K., Coxall, H. K., O'Regan, M., Nilsson, J., Caballero, R., & de Boer, A. M. (2019). Arctic closure as a trigger for Atlantic overturning at the Eocene-Oligocene Transition. *Nature Communications*, *10*(1), 3797. https://doi.org/10.1038/s41467-019-11828-z

Ionita, M., Scholz, P., Lohmann, G., Dima, M., & Prange, M. (2016). Linkages between atmospheric blocking, sea ice export through Fram Strait and the Atlantic Meridional Overturning Circulation. *Scientific Reports*, *6*(1), 32881. https://doi.org/10.1038/srep32881

Jackson, L. C., & Wood, R. A. (2018). Timescales of AMOC decline in response to fresh water forcing. *Climate Dynamics*, *51*(4), 1333–1350. https://doi.org/10.1007/s00382-017-3957-6

Jacobs, S. S. (2004). Bottom water production and its links with the thermohaline circulation. *Antarctic Science*, *16*(4), 427–437. https://doi.org/10.1017/S095410200400224X

Jakobsson, M., Backman, J., Rudels, B., Nycander, J., Frank, M., Mayer, L., et al. (2007). The early Miocene onset of a ventilated circulation regime in the Arctic Ocean. *Nature*, *447*(7147), 986–990. https://doi.org/10.1038/nature05924

Jeandel, C., Bishop, J. K., & Zindler, A. (1995). Exchange of neodymium and its isotopes between seawater and small and large particles in the Sargasso Sea. *Geochimica et Cosmochimica Acta*, *59*(3), 535–547. https://doi.org/10.1016/0016-7037(94)00367-U

Jiang, R., & Yang, H. (2021). Roles of the Rocky Mountains in the Atlantic and Pacific meridional overturning circulations. *Journal of Climate*, *34*(16), 6691–6703. https://doi.org/10.1175/JCLI-D-20-0819.1

Jokat, W., Lehmann, P., Damaske, D., & Bradley Nelson, J. (2016). Magnetic signature of North-East Greenland, the Morris Jesup Rise, the Yermak Plateau, the central Fram Strait: Constraints for the rift/drift history between Greenland and Svalbard since the Eocene. *Tectonophysics*, *691*, 98–109. https://doi.org/10.1016/j.tecto.2015.12.002

Karas, C., Nürnberg, D., Bahr, A., Groeneveld, J., Herrle, J. O., Tiedemann, R., & deMenocal, P. B. (2017). Pliocene oceanic seaways and global climate. *Scientific Reports*, *7*(1), 39842. https://doi.org/10.1038/srep39842

Kelley, M., Schmidt, G. A., Nazarenko, L. S., Bauer, S. E., Ruedy, R., Russell, G. L., et al. (2020). GISS-E2.1: Configurations and Climatology. *Journal of Advances in Modeling Earth Systems*, *12*(8), e2019MS002025. https://doi.org/10.1029/2019MS002025

Kender, S., Bogus, K. A., Cobb, T. D., & Thomas, D. J. (2018). Neodymium evidence for increased Circumpolar deep water flow to the North Pacific during the Middle Miocene Climate Transition. *Paleoceanography and Paleoclimatology*, *33*(7), 672–682. https://doi.org/10.1029/2017PA003309

Kirillova, V., Osborne, A. H., Störling, T., & Frank, M. (2019). Miocene restriction of the Pacific-North Atlantic throughflow strengthened Atlantic overturning circulation. *Nature Communications*, *10*(1), 4025. https://doi.org/10.1038/s41467-019-12034-7

Knorr, G., Butzin, M., Micheels, A., & Lohmann, G. (2011). A warm Miocene climate at low atmospheric CO_2 levels. *Geophysical Research Letters*, *38*(20), L20701. https://doi.org/10.1029/2011GL048873

Knorr, G., & Lohmann, G. (2014). Climate warming during Antarctic ice sheet expansion at the Middle Miocene transition. *Nature Geoscience*, *7*(5), 376–381. https://doi.org/10.1038/ngeo2119

Krapp, M., & Jungclaus, J. H. (2011). The Middle Miocene climate as modelled in an atmosphere-ocean-biosphere model. *Climate of the Past*, *7*(4), 1169–1188. https://doi.org/10.5194/cp-7-1169-2011

Kristoffersen, Y. (1990). On the tectonic evolution and paleoceanographic significance of the Fram Strait gateway. In U. Bleil & J. Thiede (Eds.), *Geological History of the Polar Oceans: Arctic versus Antarctic* (pp. 63–76). Springer. https://doi.org/10.1007/978-94-009-2029-3_4

Kroopnick, P. M. (1985). The distribution of ^{13}C of ΣCO_2 in the world oceans. *Deep-Sea Research, Part A: Oceanographic Research Papers*, *32*(1), 57–84. https://doi.org/10.1016/0198-0149(85)90017-2

Langton, S. J., Rabideaux, N. M., Borrelli, C., & Katz, M. E. (2016). Southeastern Atlantic deep-water evolution during the late-middle Eocene to earliest Oligocene (Ocean Drilling Program Site 1263 and Deep Sea Drilling Project Site 366). *Geosphere*, *12*(3), 1032–1047. https://doi.org/10.1130/GES01268.1

Lear, C. H., Elderfield, H., & Wilson, P. A. (2000). Cenozoic deep-sea temperatures and global ice volumes from Mg/Ca in benthic foraminiferal calcite. *Science*, *287*(5451), 269–272. https://doi.org/10.1126/science.287.5451.269

Levitus, S., & Boyer, T. (1994). *World Ocean Atlas 1994, vol. 4, Temperature*, *NOAA Atlas NESDIS 4*. National Oceanic and Atmospheric Administration.

Levitus, S., Burgett, R., & Boyer, T. P. (1994). World Ocean Atlas 1994, *Salinity* (Vol. 3).

Li, F., Lozier, M. S., & Johns, W. E. (2017). Calculating the meridional volume, heat, and freshwater transports from an observing system in the subpolar North Atlantic: Observing system simulation experiment. *Journal of Atmospheric and Oceanic Technology*, *34*(7), 1483–1500. https://doi.org/10.1175/JTECH-D-16-0247.1

Lunt, D. J., Farnsworth, A., Loptson, C., Foster, G. L., Markwick, P., O'Brien, C. L., et al. (2016). Palaeogeographic controls on climate and proxy interpretation. *Climate of the Past*, *12*(5), 1181–1198. https://doi.org/10.5194/cp-12-1181-2016

Lunt, D. J., Valdes, P. J., Haywood, A., & Rutt, I. C. (2008). Closure of the Panama Seaway during the Pliocene: Implications for climate and Northern Hemisphere glaciation. *Climate Dynamics*, *30*(1), 1–18. https://doi.org/10.1007/s00382-007-0265-6

Madole, R. F., Bradley, W. C., Loewenherz, D. S., Ritter, D. F., Rutter, N. W., & Thorn, C. E. (1987). Rocky Mountains. In W. L. Graf (Ed.), *Geomorphic Systems of North America* (Vol. 2, pp. 211–257). Geological Society of America. https://doi.org/10.1130/DNAG-CENT-v2.211

Maffre, P., Ladant, J.-B., Donnadieu, Y., Sepulchre, P., & Goddéris, Y. (2018). The influence of orography on modern ocean circulation. *Climate Dynamics*, *50*(3), 1277–1289. https://doi.org/10.1007/s00382-017-3683-0

Markwick, P. J. (2007). In M. Williams, A. M. Haywood, F. J. Gregory, & D. N. Schmidt (Eds.), *Deep-Time Perspectives on Climate Change: Marrying the Signal from Computer Models and Biological Proxies* (pp. 251–312). The Geological Society. https://doi.org/10.1017/S0954102008001600

Marshall, J., & Schott, F. (1999). Open-ocean convection: Observations, theory, and models. *Reviews of Geophysics*, *37*(1), 1–64. https://doi.org/10.1029/98rg02739

Martin, E. E., & Scher, H. D. (2004). Preservation of seawater Sr and Nd isotopes in fossil fish teeth: Bad news and good news. *Earth and Planetary Science Letters*, *220*(1), 25–39. https://doi.org/10.1016/S0012-821X(04)00030-5

McKinley, C. C., Thomas, D. J., LeVay, L. J., & Rolewicz, Z. (2019). Nd isotopic structure of the Pacific Ocean 40–10 Ma, and evidence for the reorganization of deep North Pacific Ocean circulation between 36 and 25 Ma. *Earth and Planetary Science Letters*, *521*, 139–149. https://doi.org/10.1016/j.epsl.2019.06.009

Micheels, A., Bruch, A. A., Eronen, J., Fortelius, M., Harzhauser, M., Utescher, T., & Mosbrugger, V. (2011). Analysis of heat transport mechanisms from a Late Miocene model experiment with a fully-coupled atmosphere–ocean general circulation model. *Palaeogeography, Palaeoclimatology, Palaeoecology*, *304*(3), 337–350. https://doi.org/10.1016/j.palaeo.2010.09.021

Micheels, A., Bruch, A. A., & Mosbrugger, V. (2009). Miocene climate modelling sensitivity experiments for different CO_2 concentrations. *Palaeontologia Electronica*, *12*(2), 1–19.

Miller, K., Fairbanks, R., & Thomas, E. (1987). Benthic foraminiferal carbon isotopic records and the development of abyssal circulation in the eastern North Atlantic.

Miller, K. G., Browning, J. V., Schmelz, W. J., Kopp, R. E., Mountain, G. S., & Wright, J. D. (2020). Cenozoic sea-level and cryospheric evolution from deep-sea geochemical and continental margin records. *Science Advances*, *6*(20), eaaz1346. https://doi.org/10.1126/sciadv.aaz1346

Miller, K. G., & Tucholke, B. E. (1983). Development of Cenozoic abyssal circulation south of the Greenland-Scotland Ridge. In *Structure and development of the Greenland-Scotland Ridge* (pp. 549–589). Springer.

Montes, C., Bayona, G., Cardona, A., Buchs, D. M., Silva, C., Morón, S., et al. (2012). Arc-continent collision and orocline formation: Closing of the Central American seaway. *Journal of Geophysical Research*, *117*(B4), B04105. https://doi.org/10.1029/2011jb008959

Montes, C., Cardona, A., Jaramillo, C., Pardo, A., Silva, J., Valencia, V., et al. (2015). Middle Miocene closure of the Central American seaway. *Science*, *348*(6231), 226–229. https://doi.org/10.1126/science.aaa2815

Morrill, C., LeGrande, A. N., Renssen, H., Bakker, P., & Otto-Bliesner, B. L. (2013). Model sensitivity to North Atlantic freshwater forcing at 8.2 ka. *Climate of the Past*, *9*(2), 955–968. https://doi.org/10.5194/cp-9-955-2013

Müller-Michaelis, A., & Uenzelmann-Neben, G. (2014). Development of the Western Boundary Undercurrent at Eirik Drift related to changing climate since the early Miocene. *Deep Sea Research Part I: Oceanographic Research Papers*, *93*, 21–34. https://doi.org/10.1016/j.dsr.2014.07.010

Müller-Michaelis, A., Uenzelmann-Neben, G., & Stein, R. (2013). A revised Early Miocene age for the instigation of the Eirik Drift, offshore southern Greenland: Evidence from high-resolution seismic reflection data. *Marine Geology*, *340*, 1–15. https://doi.org/10.1016/j.margeo.2013.04.012

Naik, T. (2025). trushanaik/MioMIP1-Ocean-Intercomparison: First release (Version 1.0) [Software]. *Zenodo*. https://doi.org/10.5281/zenodo.15190395

Naik, T., de Boer, A., Burls, N., Bradshaw, C., Donnadieu, Y., Farnsworth, A., et al. (2025). Ocean model output from MioMIP1 climate simulations of the early and middle Miocene [Dataset] (Version 1). *Bolin Centre Database*. https://doi.org/10.17043/naik-2025-miomip1-moc-1

O'Dea, A., Lessios, H. A., Coates, A. G., Eytan, R. I., Restrepo-Moreno, S. A., Cione, A. L., et al. (2016). Formation of the Isthmus of Panama. *Science Advances*, *2*(8), e1600883. https://doi.org/10.1126/sciadv.1600883

O'Regan, M., Williams, C. J., Frey, K. E., & Jakobsson, M. (2011). A synthesis of the long-term paleoclimatic evolution of the Arctic. *Oceanography*, *24*(3), 66–80. https://doi.org/10.5670/oceanog.2011.57

Osborne, A. H., Hathorne, E. C., Böning, P., Groeneveld, J., Pahnke, K., & Frank, M. (2019). Late Pliocene and Early Pleistocene variability of the REE and Nd isotope composition of Caribbean bottom water: A record of changes in sea level and terrestrial inputs during the final stages of Central American Seaway closure. *Paleoceanography and Paleoclimatology*, *34*(12), 2067–2079. https://doi.org/10.1029/2019PA003654

Osborne, A. H., Newkirk, D. R., Groeneveld, J., Martin, E. E., Tiedemann, R., & Frank, M. (2014). The seawater neodymium and lead isotope record of the final stages of Central American Seaway closure. *Paleoceanography*, *29*(7), 715–729. https://doi.org/10.1002/2014pa002676

Pellichero, V., Sallée, J.-B., Schmidtko, S., Roquet, F., & Charrassin, J.-B. (2017). The ocean mixed layer under Southern Ocean sea-ice: Seasonal cycle and forcing. *Journal of Geophysical Research: Oceans*, *122*(2), 1608–1633. https://doi.org/10.1002/2016JC011970

Pillot, Q., Donnadieu, Y., Sarr, A. C., Ladant, J. B., & Suchéras-Marx, B. (2022). Evolution of Ocean circulation in the North Atlantic Ocean during the Miocene: Impact of the Greenland ice sheet and the Eastern Tethys Seaway. *Paleoceanography and Paleoclimatology*, *37*(8), e2022PA004415. https://doi.org/10.1029/2022PA004415

Poblete, F., Dupont-Nivet, G., Licht, A., Van Hinsbergen, D. J., Roperch, P., Mihalynuk, M., et al. (2021). Towards interactive global paleo-geographic maps, new reconstructions at 60, 40 and 20 Ma. *Earth-Science Reviews*, *214*, 103508. https://doi.org/10.1016/j.earscirev.2021.103508

Poore, H. R., Samworth, R., White, N. J., Jones, S. M., & McCave, I. N. (2006). Neogene overflow of Northern Component Water at the Greenland-Scotland Ridge. *Geochemistry, Geophysics, Geosystems*, *7*(6), Q06010. https://doi.org/10.1029/2005GC001085

Pöppelmeier, F., Scheen, J., Jeltsch-Thömmes, A., & Stocker, T. F. (2021). Simulated stability of the Atlantic Meridional Overturning Circulation during the Last Glacial Maximum. *Climate of the Past*, *17*(2), 615–632. https://doi.org/10.5194/cp-17-615-2021

Potter, P. E., & Szatmari, P. (2009). Global Miocene tectonics and the modern world. *Earth-Science Reviews*, *96*(4), 279–295. https://doi.org/10.1016/j.earscirev.2009.07.003

Prange, M., Lohmann, G., & Gerdes, R. (1997). Sensitivity of the thermohaline circulation for different climates—Investigations with a simple atmosphere–ocean model. *Palaeoclimates*, *2*(1), 71–99.

Putrasahan, D. A., Lohmann, K., von Storch, J.-S., Jungclaus, J. H., Gutjahr, O., & Haak, H. (2019). Surface flux drivers for the slowdown of the Atlantic meridional overturning circulation in a high-resolution global coupled climate model. *Journal of Advances in Modeling Earth Systems*, *11*(5), 1349–1363. https://doi.org/10.1029/2018MS001447

Rae, J. W. B., Zhang, Y. G., Liu, X., Foster, G. L., Stoll, H. M., & Whiteford, R. D. M. (2021). Atmospheric CO_2 over the past 66 million years from marine archives. *Annual Review of Earth and Planetary Sciences*, *49*(1), 609–641. https://doi.org/10.1146/annurev-earth-082420-063026

Ravelo, A., & Hillaire-Marcel, C. (2007). The use of oxygen and carbon isotopes of foraminifera in paleoceanography. In *Developments in Marine Geology* (Vol. 10, pp. S1572–S5480). Elsevier BV.

Rebesco, M., Hernández-Molina, F. J., Van Rooij, D., & Wåhlin, A. (2014). Contourites and associated sediments controlled by deep-water circulation processes: State-of-the-art and future considerations. *Marine Geology*, *352*, 111–154. https://doi.org/10.1016/j.margeo.2014.03.011

Rintoul, S. R., Hughes, C. W., & Olbers, D. (2001). Chapter 4.6 The Antarctic Circumpolar Current system. In G. Siedler, J. Church, & J. Gould (Eds.), *International Geophysics* (Vol. 77, pp. 271–302). Academic Press. Retrieved from https://www.sciencedirect.com/science/article/pii/S0074614201801248

Sangiorgi, F., Brumsack, H.-J., Willard, D. A., Schouten, S., Stickley, C. E., O'Regan, M., et al. (2008). A 26 million year gap in the central Arctic record at the greenhouse-icehouse transition: Looking for clues. *Paleoceanography*, *23*(1), PA1S04. https://doi.org/10.1029/2007PA001477

Scher, H. D., & Martin, E. E. (2008). Oligocene deep water export from the North Atlantic and the development of the Antarctic Circumpolar Current examined with neodymium isotopes. *Paleoceanography*, *23*(1), PA1205. https://doi.org/10.1029/2006PA001400

Schmittner, A., Silva, T. A. M., Fraedrich, K., Kirk, E., & Lunkeit, F. (2011). Effects of mountains and ice sheets on global ocean circulation. *Journal of Climate*, *24*(11), 2814–2829. https://doi.org/10.1175/2010JCLI3982.1

Scotese, C. R., & Wright, N. (2018). PALEOMAP paleodigital elevation models (PaleoDEMS) for the Phanerozoic. *Paleomap Project*.

Sijp, W. P., von der Heydt, A. S., Dijkstra, H. A., Flögel, S., Douglas, P. M. J., & Bijl, P. K. (2014). The role of ocean gateways on cooling climate on long time scales. *Global and Planetary Change*, *119*, 1–22. https://doi.org/10.1016/j.gloplacha.2014.04.004

Sinha, B., Blaker, A. T., Hirschi, J. J.-M., Bonham, S., Brand, M., Josey, S., et al. (2012). Mountain ranges favour vigorous Atlantic meridional overturning. *Geophysical Research Letters*, *39*(2), L02705. https://doi.org/10.1029/2011GL050485

Sjostrom, D. J., Hren, M. T., Horton, T. W., Waldbauer, J. R., Chamberlain, C. P., Willett, S. D., et al. (2006). Stable isotopic evidence for a pre–late Miocene elevation gradient in the Great Plains–Rocky Mountain region, USA. In *Tectonics, Climate, and Landscape Evolution* (Vol. 398). Geological Society of America. https://doi.org/10.1130/2006.2398(19)

Störz, M., Jokat, W., Knorr, G., & Lohmann, G. (2017). Threshold in North Atlantic-Arctic Ocean circulation controlled by the subsidence of the Greenland-Scotland Ridge. *Nature Communications*, *8*(1), 15681. https://doi.org/10.1038/ncomms15681

Steinthorsdottir, M., Coxall, H. K., de Boer, A. M., Huber, M., Barbolini, N., Bradshaw, C. D., et al. (2021). The Miocene: The future of the past. *Paleoceanography and Paleoclimatology*, *36*(4), e2020PA004037. https://doi.org/10.1029/2020PA004037

Steph, S., Tiedemann, R., Prange, M., Groeneveld, J., Nürnberg, D., Reuning, L., et al. (2006). Changes in Caribbean surface hydrography during the Pliocene shoaling of the Central American Seaway. *Paleoceanography*, *21*(4), PA4221. https://doi.org/10.1029/2004PA001092

Stephens, C., & Levitus, S. (2002). World Ocean Atlas 2001, *Temperature* (Vol. *1*).

Stow, D., & Smillie, Z. (2020). Distinguishing between deep-water sediment facies: Turbidites, contourites and hemipelagites. *Geosciences*, *10*(2), 68. https://doi.org/10.3390/geosciences10020068

Stow, D. A. V., Faugères, J.-C., Howe, J. A., Pudsey, C. J., & Viana, A. R. (2002). Bottom currents, contourites and deep-sea sediment drifts: Current state-of-the-art. *Geological Society, London, Memoirs*, *22*(1), 7–20. https://doi.org/10.1144/GSL.MEM.2002.022.01.02

Su, B., Jiang, D., Zhang, R., Sepulchre, P., & Ramstein, G. (2018). Difference between the North Atlantic and Pacific meridional overturning circulation in response to the uplift of the Tibetan Plateau. *Climate of the Past*, *14*(6), 751–762. https://doi.org/10.5194/cp-14-751-2018

Sun, J., Sheykh, M., Ahmadi, N., Cao, M., Zhang, Z., Tian, S., et al. (2021). Permanent closure of the Tethyan Seaway in the northwestern Iranian Plateau driven by cyclic sea-level fluctuations in the late Middle Miocene. *Palaeogeography, Palaeoclimatology, Palaeoecology*, *564*, 110172. https://doi.org/10.1016/j.palaeo.2020.110172

Tachikawa, K., Jeandel, C., & Roy-Barman, M. (1999). A new approach to the Nd residence time in the ocean: The role of atmospheric inputs. *Earth and Planetary Science Letters*, *170*(4), 433–446. https://doi.org/10.1016/S0012-821X(99)00127-2

Thomas, D. J., Korty, R., Huber, M., Schubert, J. A., & Haines, B. (2014). Nd isotopic structure of the Pacific Ocean 70–30 Ma and numerical evidence for vigorous ocean circulation and ocean heat transport in a greenhouse world. *Paleoceanography*, *29*(5), 454–469. https://doi.org/10.1002/2013pa002535

Thomas, D.J., & Via, R. K. (2007). Neogene evolution of Atlantic thermohaline circulation: Perspective from Walvis Ridge, southeastern Atlantic Ocean. *Paleoceanography*, *22*(2), PA2212. https://doi.org/10.1029/2006PA001297

Toucanne, S., Soulet, G., Freslon, N., Silva Jacinto, R., Dennielou, B., Zaragosi, S., et al. (2015). Millennial-scale fluctuations of the European Ice Sheet at the end of the last glacial, and their potential impact on global climate. *Quaternary Science Reviews*, *123*, 113–133. https://doi.org/10.1016/j.quascirev.2015.06.010

Treguier, A. M., De Boyer Montégut, C., Bozec, A., Chassignet, E. P., Fox-Kemper, B., McC. Hogg, A., et al. (2023). The mixed-layer depth in the Ocean Model Intercomparison Project (OMIP): Impact of resolving mesoscale eddies. *Geoscientific Model Development*, *16*(13), 3849–3872. https://doi.org/10.5194/gmd-16-3849-2023

Uenzelmann-Neben, G., & Gruetzner, J. (2018). Chronology of Greenland Scotland Ridge overflow: What do we really know? *Marine Geology*, *406*, 109–118. https://doi.org/10.1016/j.margeo.2018.09.008

Våge, K., Pickart, R. S., Thierry, V., Reverdin, G., Lee, C. M., Petrie, B., et al. (2009). Surprising return of deep convection to the subpolar North Atlantic Ocean in winter 2007–2008. *Nature Geoscience*, *2*(1), 67–72. https://doi.org/10.1038/ngeo382

Via, R. K., & Thomas, D. J. (2006). Evolution of Atlantic thermohaline circulation: Early Oligocene onset of deep-water production in the North Atlantic. *Geology*, *34*(6), 441. https://doi.org/10.1130/G22545.1

von der Heydt, A., & Dijkstra, H. A. (2006). Effect of ocean gateways on the global ocean circulation in the late Oligocene and early Miocene. *Paleoceanography*, *21*(1), PA1011. https://doi.org/10.1029/2005PA001149

Waddell, L. M., & Moore, T. C. (2008). Salinity of the Eocene Arctic Ocean from oxygen isotope analysis of fish bone carbonate. *Paleoceanography*, *23*(1), PA1S12. https://doi.org/10.1029/2007PA001451

Wang, C., Dai, J., Zhao, X., Li, Y., Graham, S. A., He, D., et al. (2014). Outward-growth of the Tibetan Plateau during the Cenozoic: A review. *Tectonophysics*, *621*, 1–43. https://doi.org/10.1016/j.tecto.2014.01.036

Wang, C., Li, X., Hu, X., & Jansa, L. F. (2002). Latest marine horizon north of Qomolangma (Mt Everest): Implications for closure of Tethys seaway and collision tectonics. *Terra Nova*, *14*(2), 114–120. https://doi.org/10.1046/j.1365-3121.2002.00399.x

Wang, H., Legg, S., & Hallberg, R. (2018). The effect of Arctic freshwater pathways on North Atlantic convection and the Atlantic meridional overturning circulation. *Journal of Climate*, *31*(13), 5165–5188. https://doi.org/10.1175/JCLI-D-17-0629.1

Wang, H., Liu, W., Lu, H., Zhang, Y., Liang, Y., He, Y., et al. (2023). Oxygenated deep waters fed early Atlantic overturning circulation upon Antarctic glaciation. *Nature Geoscience*, *16*(11), 1014–1019. https://doi.org/10.1038/s41561-023-01292-2

Webb, S. D. (2006). The Great American Biotic Interchange: Patterns and processes. *Annals of the Missouri Botanical Garden*, *93*(2), 245–257. https://doi.org/10.3417/0026-6493(2006)93[245:tgabip]2.0.co;2

Wen, Q., & Yang, H. (2020). Investigating the role of the Tibetan Plateau in the formation of Pacific meridional overturning circulation. *Journal of Climate*, *33*(9), 3603–3617. https://doi.org/10.1175/JCLI-D-19-0206.1

Wolfe, J. A., Schorn, H. E., Forest, C. E., & Molnar, P. (1997). Paleobotanical evidence for high altitudes in Nevada during the Miocene. *Science*, *276*(5319), 1672–1675. https://doi.org/10.1126/science.276.5319.1672

Woodruff, F., & Savin, S. M. (1989). Miocene deepwater oceanography. *Paleoceanography*, *4*(1), 87–140. https://doi.org/10.1029/pa004i001p00087

Wright, J. D., & Miller, K. G. (1996). Control of North Atlantic deep water circulation by the Greenland-Scotland Ridge. *Paleoceanography*, *11*(2), 157–170. https://doi.org/10.1029/95PA03696

Wright, J. D., Miller, K. G., & Fairbanks, R. G. (1992). Early and Middle Miocene stable isotopes: Implications for Deepwater circulation and climate. *Paleoceanography*, *7*(3), 357–389. https://doi.org/10.1029/92PA00760

Wright, N. M., Scher, H. D., Seton, M., Huck, C. E., & Duggan, B. D. (2018). No change in Southern Ocean circulation in the Indian Ocean from the Eocene through late Oligocene. *Paleoceanography and Paleoclimatology*, *33*(2), 152–167. https://doi.org/10.1002/2017PA003238

Yang, H., Jiang, R., Wen, Q., Liu, Y., Wu, G., & Huang, J. (2024). The role of mountains in shaping the global meridional overturning circulation. *Nature Communications*, *15*(1), 2602. https://doi.org/10.1038/s41467-024-46856-x

Yang, H., Li, Q., Wang, K., Sun, Y., & Sun, D. (2015). Decomposing the meridional heat transport in the climate system. *Climate Dynamics*, *44*(9), 2751–2768. https://doi.org/10.1007/s00382-014-2380-5

Zhang, Y., De Boer, A. M., Lunt, D. J., Hutchinson, D. K., Ross, P., Van De Flierdt, T., et al. (2022). Early Eocene ocean meridional overturning circulation: The roles of atmospheric forcing and strait geometry. *Paleoceanography and Paleoclimatology*, *37*(3), e2021PA004329. https://doi.org/10.1029/2021PA004329

Zhang, Z., Nisancioglu, K. H., Flatøy, F., Bentsen, M., Bethke, I., & Wang, H. (2011). Tropical seaways played a more important role than high latitude seaways in Cenozoic cooling. *Climate of the Past*, *7*(3), 801–813. https://doi.org/10.5194/cp-7-801-2011

Zhu, C., Meng, J., Hu, Y., Wang, C., & Zhang, J. (2019). East-central Asian climate evolved with the northward migration of the high Proto-Tibetan Plateau. *Geophysical Research Letters*, *46*(14), 8397–8406. https://doi.org/10.1029/2019GL082703

Zhu, J., Poulsen, C. J., & Tierney, J. E. (2019). Simulation of Eocene extreme warmth and high climate sensitivity through cloud feedbacks. *Science Advances*, *5*(9), eaax1874. https://doi.org/10.1126/sciadv.aax1874